ResearchOnline@JCU

JAMES COOK UNIVERSITY AUSTRALIA

This is the author-created version of the following work:

Chalak Qazani, Mohamad Reza, Pourmostaghimi, Vahid, Moayyedian, Mehdi, and Pedrammehr, Siamak (2022) ***Estimation of tool--chip contact length using optimized machine learning in orthogonal cutting.*** **Engineering Applications of Artificial Intelligence, 114 .**

Access to this file is available from:

https://researchonline.jcu.edu.au/86736/

© 2022 Elsevier Ltd. All rights reserved. AAM may be made open access in an Institutional Repository under a CC BY-NC-ND license after a 24 month embargo.

Please refer to the original source for the final version of this work:

https://doi.org/10.1016/j.engappai.2022.105118

Estimation of Tool–Chip Contact Length Using Optimized Machine Learning in Orthogonal Cutting

Mohammad Reza Chalak Qazani[a,1], Vahid Pourmostaghimi[b], Mehdi Moayyedian[c], Siamak Pedrammehr[d]

[a] *Institute for Intelligent Systems Research and Innovation, Deakin University, Geelong, VIC 3216, Australia*

[b] *Department of Manufacturing and Production Engineering, Faculty of Mechanical Engineering, University of Tabriz, Tabriz, Iran*

[c] *College of Engineering and Technology, American University of the Middle East, Kuwait*

[d] *Faculty of Mechanical Engineering, University of Tabriz, Tabriz, Iran*

A Research Paper

Submitted to

Engineering Applications of Artificial Intelligence

2022

[1] Corresponding author:
Email addresses: m.r.chalakqazani@gmail.com (*Mohammad Reza Chalak Qazani*)

Abstract

Tool-chip contact length has a significant effect on the various characteristics of metal cutting, including cutting pressures, chip formation, tool wear, tool life, and cutting temperatures. It should be added that there is a direct relationship between the tool–chip contact length and secondary shear zone thickness in the metal cutting process. The cutting force and shear zone temperature decrease by the reduction of tool–chip contact length. In addition, the tool–chip contact length affects the tool life and workpiece surface roughness. Lots of researchers have conducted extensive research to calculate the tool-chip contact length using mathematical or machine learning methods. The main objective of this study is to calculate the tool–chip contact length using a highly advanced machine learning method without any time-consuming and expensive experiments. However, an adaptive network-based fuzzy inference system (ANFIS) is not used yet in the prediction of the tool–chip contact length. In this study, we proposed the ANFIS to predict the tool–chip contact length for the first time in orthogonal cutting using depth of cut, feed-rate, and cutting speed as inputs of the proposed model. As the second contribution of this study, three evolutionary-based optimization techniques, including genetic algorithm, particle swarm optimization, and grey wolf optimization, as well as global-based Bayesian optimization, are employed to select the optimal hyperparameters of the proposed ANFIS model known as GA-ANFIS, PSO-ANFIS, GWO-ANFIS, and B-ANFIS, respectively. The proposed methods are designed and developed in MATLAB software to be compared with the previous method using genetic programming (GP). The outcomes of this research demonstrate that the GWO-ANFIS can decrease the mean square error between the actual and predicted tool-chip contact length of 15.60%, 3.67%, 89.75%, and 92.17% in comparison with those of GA-ANFIS, PSO-ANFIS, B-ANFIS, and GP, respectively. In addition, the fuzzy logic rule surface of the GWO-ANFIS shows 57.20%, 30.95%, and 11.85% dependency of tool-chip contact length to cutting speed, feed-rate, and depth of cut as the inputs of the orthogonal cutting process, respectively.

Keywords: Tool–chip contact length; optimization; adaptive network-based fuzzy inference system.

I. INTRODUCTION

Tool-chip contact length occurs when a continuous chip contacts the tool rake face. The chip formation zone geometry is defined to evaluate the heat in the secondary deformation zone. The pattern of the temperature and cutting force is predicted via the contact stress distribution and contact feature to calculate the tool strength for tool selection and to control the manufacturing process. Many different investigations have been performed in the field. Poletika [1] conducted several experiments with a variety of materials and machining conditions, including carbon steels and stainless steels, armco-iron, various bronzes and coppers with varying hardness. He discovered that tool–chip contact length is directly relevant to the undeformed thickness of the chip and the chip compression ratio. Friedman and Lenz [2] discovered the wide variation in tool-chip contact length for machining of steel using different grades of the tool by fixing the other cutting variables. Kato *et al.* [3] observed that the tool-chip contact length is twice the deformed chip thickness when using the split tool technique. Sadik and Lindström [4] discovered a correlation between the different parameters of three-dimensional cutting, including coating material, work material, flank wear, tool temperature, cutting force and tool-chip contact length. Sadik and Lindström [5] studied the influence of the restricted contact length on the performance of the tool. They discovered that less tool-chip contact length decreases the flank wear of the tool. Abukhshim *et al.* [6] investigated the length of tool-chip contact during high-speed machining of EN19 steel. Sutter [7] determined the contact length for a variety of workpiece materials for an orthogonal cutting method. His proposed model linked the tool-chip contact length to the cutting speed and the workpiece's material. However, the shape of the tool, the feed-rate, and the friction at the interface proportionally affect the tool-chip contact length. Sutter [7] investigated the contact length using tools with various rake angles (+50 and -50) and discovered a large dispersion for the normalized length of contact. Wherein the mentioned method, the rake angle was established after choosing a tool holder or solid tool, while inserting the cutting conditions. Korkut and Donertas [8] studied the relationship between the selected cutting speed and feed-rate on obtained surface roughness, resulting in cutting force and tool–chip contact length during the milling operation. Iqbal *et al.* [9] developed contact length modelling for both materials

that apply to a wide variety of cutting speeds. Decreased coefficients of friction are seen at high cutting speeds [10]. Mikołajczyk [11] investigated the influence of the thickness cutting layer on the surface roughness of the workpiece during metal cutting. Consequently, friction and cutting parameters were included in studies to evaluate the influences of cutting speed on contact length. This is critical because the friction coefficient in industrial machining is dictated by the tool and workpiece materials employed and fluctuates according to the cutting conditions. Mohapatra *et al.* [12] observed that cutting speed rose from 30 to 50 (m/min), and the chip–tool contact length reduced, resulting in a smaller sliding zone and a larger sticking zone. Ortiz-de-Zarate *et al.* [13] employed partially restricted contact length tools to map the normal stress distribution and friction on the rake face during orthogonal cutting trials. Zhang *et al.* [14] divided the tool-chip contact interface during quasi-intermittent vibration-assisted swing cutting using the two-zone analytical modelling approach. They observed that for cutting speeds varying from 7.85 to 11.78 (m/min), the actual and theoretical cutting force inaccuracy of quasi-intermittent vibration-assisted swing cutting was less than 15%.

With advancements in artificial intelligence, data-driven strategies for mapping exceedingly nonlinear and complicated data have attracted novel interest in a range of research fields, including material microstructure, energy, inorganic nanomaterials, and manufacturing, to name a few [15, 16]. Although these data-driven models are not based on process physics, they can provide models with superior accuracy to conventional mechanistic modellings [17, 18]. Zadshakoyan and Pourmostaghimi [19] analysed the mathematical connection between tool–chip contact length and cutting parameters using genetic programming (GP). Due to the system's complexity, their proposed solution proved incapable of producing accurate results. Zadshakoyan and Pourmostaghimi [20] presented a genetic equation for tool wear based on differences in the radius of the chips produced during the turning operation. They combined a variety of processes, including manufacturing technology, evolutionary approaches, control and measurement technology, and the associated software and hardware [20]. They also developed a novel intelligence-based approach for determining optimal cutting indexes in AISI D2 hard turning. It examined an intelligent method for

maximizing tool life and material removal rate during AISI D2 finish hard turning processes [21]. Nguyen-Le *et al.* [22] used long short-term memory (LSTM) hidden Markov model to forecast crack propagation. They discovered that the hybrid LSTM and Markov model reaches more accuracy than LSTM. Xu *et al.* [23] developed a neuro-fuzzy adaptive inference system for the prediction of energy usage and surface quality during high-speed milling. Fuzzy inference system has been used in engineering topics such as aerospace [24], motion platform control mechanism [25] and motion cueing algorithm [26]. In EN31 steel machining with changeable cutting parameters, Setia and Chauhan [27] developed a feedforward neural network to anticipate cutting force and tool tip temperature. Charalampous [28] utilized a range of machine learning techniques to estimate milling cutting forces, including support vector regression, k-nearest neighbour, polynomial regression and random forest. Annapurna and Mounika Yesaswini [29] developed an improved version of the Hungarian algorithm for solving the unbalanced assignments. Tran-Ngoc *et al.* [30] identified the damage using optimised MLP based on a metaheuristic algorithm, including GA and cuckoo search. The results prove the efficiency of the proposed method compared to nonoptimized MLP. Wang *et al.* [31] used the deep learning method to recognise the profile via automatic laser. Their proposed fast-tracking method solves the profile measurement in various types of laser stripes. Qazani *et al.* [32] used the hybrid fuzzy inference system and neural network in designing the optimal washout filter in the motion simulator platform. Later, Qazani *et al.* [33] used the metaheuristic optimised machine learning methods (ANFIS, MLP and LSTM) for extracting the optimal designing parameter of the 3-2-1 fixture.

The main motivation of this study compared to the previous methods is the development of machine learning models with the ability to handle complex systems with limited datasets. The calculation of the tool-chip contact length needs to be handled using the experiment, which is very time-consuming and expensive. This study proposed an effective adaptive network-based fuzzy inference system (ANFIS) model to predict the tool–chip contact length based on the machining parameters, including depth of cut, feed-rate, and cutting speed. The samples are gathered using the lathe machine operation of the AISI4140 as a workpiece and a cemented uncoated carbide as a tool using 44 different machining parameters, including depth of cut, feed-

rate, and cutting speed. Then, datasets are recorded by measuring the contact length between the tool and the chip using an optical microscope equipped with image processing software. The dataset is divided into 80% and 20% for training and testing purposes of the investigated ANFIS model. The hyperparameters of the ANFIS, including initial FIS, epoch number, initial step size, decreasing rate of step size, and increasing rate of step size, should be selected wisely to reach the higher efficiency using the proposed ANFIS model in the prediction of tool–chip contact length based on the machining parameters. Focusing on the tuning of the ANFIS hyperparameters, three evolutionary-based and one global-based optimization technique are used to extract the optimal model to predict the tool–chip contact length. Genetic algorithm (GA), particle swarm optimization (PSO), and grey wolf optimization (GWO) are our candidates for evolutionary-based optimization methodologies. GA is selected in this research as the first selected evolutionary-based algorithm because it is the oldest and best effective evolutionary algorithm in soft computing methods [34]. Also, PSO is the second evolutionary-based algorithm employed in this study because of its simplicity, applicability, fast convergence speed, and accuracy [35]. Lastly, GWO is investigated as the last evolutionary-based algorithm due to the simple structure, cheaper computational load [36], easy implementation, faster convergence speed, fewer decision variables, less number of hyperparameters, better stability, and higher robustness [37]. Additionally, the Bayesian optimization strategy, one of the most promising global optimization methods, is considered in this research for tuning the ANFIS hyperparameters [38].

The overview of the tool–chip contact length in orthogonal cutting methods are explained in the following Section. The paper's methodology, including the four investigated methods (ANFIS) with the combination of optimization techniques (GA, PSO, GWO and Bayesian), are described in Section III. The investigated methods are verified and validated in MATLAB, and the outputs are reported and discussed in Section IV. The most remarkable results are described, and the conclusions will be made in Section V.

II. Tool–Chip Contact Length in Orthogonal Cutting Methods

Tool-chip contact length is defined as the length in which the continuous produces chip remains in contact with tool rake face during chip formation. In fact, this length is measured from the tool's tip to the point that chip leaves the rake face. Since tool-chip contact length determines the characteristics of the chip formation zone, it can be said that this length affects the amount of generated heat during cutting process in the secondary deformation area over the tool rake face. On the other hand, because of the importance of generated heat in secondary shear zone and its effect on tool crater wear [39], it can be concluded that having through information about tool-chip contact characteristics and generated cutting stress in the tool's rake face makes it possible to obtain optimum cutting tool geometry in terms of cutting tool strength and tool life.

1. Theory of Tool-Chip Contact Length

The tool-chip contact length region is divided into two zones, including the plastic and elastic zones. The plastic zone (sticking region) is near the tool edge with higher shear stress. The elastic zone (sliding region) occurs at the end of contact length with low shear stress. Mikołajczyk *et al.* [40] investigated the cutting edge angle influence on minimum uncut chip thickness during the lathe machining operation of C45 steel. Fig. 1 illustrates the geometric elements of the tool–chip contact length during the orthogonal metal cutting operation. Based on the conducted work by Lee and Shaffer [41], the tool chip contact length is a function of shear angle, undeformed chip thickness and tool rake angle.

There is not a straightforward mathematical formula to relate the tool–chip contact length to the shear process in the contact zone. That is the main reason that the calculated tool–chip contact length is different for the same set of tool shapes and machining conditions. Based on the reviewed articles in this study, the majority of work in this field used the actual and undeformed chip thickness for modelling the tool–chip contact length. However, lots of data should be experimentally obtained to develop Lee and Shaffer's model [41], such as cutting force, material coefficients and shear angle. Due to the complexity and lack of a systematic method for calculation of contact length, the machine learning method is employed in this study to model the tool-

chip contact length using metal-cutting parameters, including the cutting speed, feed-rate and depth of cut. A fuzzy logic method is employed in this study as one of the highly efficient soft computing methods to achieve the task. This method will be applied to the manufacturing operation to determine tool-chip contact length with a few experimental tests.

2.Experimentation and Data collection

The configuration for workpiece machining is shown in Fig. 2. All studies were conducted in a dry environment using a CNC lathe machine. The cutting speed should not be varied during the cutting operation. Then, a large diameter workpiece is employed to avoid this phenomenon across the cutting edge. Different rational arrangements of cutting speed values v form feed-rate f and depth of cut a have been chosen in this work to construct the ANFIS model, as represented in Table 1. All experiments were performed three times, and the average obtained value for tool-chip contact length was selected in analyzing and modelling stage.

A cemented uncoated carbide insert with specification TNMA220408 and grade P20 was used in performing cutting tests and AISI4140 as a workpiece to compare the results with the previous works [19] in this field. A micrometer is employed to calculate the actual chip thickness at each trial. Cutting parameters were selected based on response surface and Taguchi methodology from values illustrated in Table 1. Therefore, the total number of 36 tests was considered, which are used in the training phase of modelling. For evaluating the accuracy of obtained model, 8 additional tests with the different cutting parameters were performed, and the corresponding tool-chip contact length was measured.

Fig. 3 illustrates the approach for measuring the tool-chip contact length via the tool using an optical microscope combined with image processing software. Fig. 4 demonstrates the contact length for the tool-chip for two different cutting conditions. In Fig. 4a, contact length of 368 (μm) for v = 55 (m/min), f = 0.2 (mm/rev), a = 2.7 (mm) was obtained. This data was taken from the testing dataset. For v = 120 (m/min), f = 0.11 (mm/rev), a = 2.1 (mm) from training dataset, the average contact length 483 (μm) was measured based on the represented results in Fig. 4b.

The images are captured using a light source microscope with a magnification of 36X equipped with imaging processing software. Captured images were sent to CLEMEX software to measure the contact length of the tool with chip. The point where the chip separates from the tool surface defines the tool-chip contact length. In other words, the distance between this defined point and the cutting edge determines the tool-chip contact length. In all measurements, this distance was measured in the vertical direction to the cutting edge.

III. METHODOLOGY

Two independent data sets were created from measurements to estimate tool–chip contact length. Feed-rate, cutting speed, and cut depth are independent input variables, and the length of contact is the output. An equation for the length of contact was generated on the training data set basis, and the resultant model's correctness was shown using fitness functions on the testing data set. The provided model's findings have also been compared with the results of previously performed research on the tool–chip contact length.

Fig. 5. shows the schematic proposed method in this paper from lath machining of the workpiece until the prediction of tool–chip contact length. According to Fig. 5-a, the process starts with machining the workpiece using a lath CNC machine with specific cutting parameters. Then, the flank wear is measured via the optical microscope combined with image processing software. The test results are recorded to be used in the proposed model for the prediction of the tool–chip contact length based on the selected machining parameters. Fig. 5b presents the implementation of our newly proposed optimized ANFIS on data for the contact length of tool–chip interface. The algorithm consists of data pre-processing to eliminate the doggy data to increase the algorithm's accuracy. Then, standardization or normalization is used to decrease the system's complexity network. The three evolutionary-based optimizations (GA, PSO and GWO) with the addition of one global optimization (Bayesian optimization method) are employed to select the optimal hyperparameters of the ANFIS to reach the lowest mean square error (MSE) as well as the highest correlation coefficient (CC) between the actual and predicted data. The data is divided into training and testing groups

to be trained via the training data and tested via the testing data. Finally, the testing data is implemented in the optimal extracted ANFIS models.

1.Data Manipulation and Preparation

Three tasks should be implemented before developing the model and applying the dataset. Initially, there are some data with minus force. These data should be removed because there are generated resulting from the malfunction of the system. Also, the out-of-range data because of the fault of the sensors should be removed before employing within the models. The second step is related to the normalization or standardization of the system to decrease the complexity of the data for a system before training. In this work, both methods are employed in the system to decrease the complexity of the network's input data and increase the accuracy of the system. The following formulation is used to calculate the standardization of the data:

$$\sigma_{x_i} = \frac{x_i - \bar{x}}{\sigma_x} \tag{1}$$

where x_i, and σ_{x_i} are the raw and standardized i^{th} input data, respectively. Also, $\bar{x}$and σ_x are the function for extracting the average and data standard deviation. Also, the normalized data is calculated as:

$$n_{x_i} = \frac{x_i - \underline{x}}{\overline{x} - \underline{x}} \tag{2}$$

where n_{x_i} is the i^{th} normalized input data. Also, $\overline{x}$and $\underline{x}$ are the functions for extracting the maximum and minimum values of the data. During the final pre-tuning process of the network, the data is divided into 80% and 20% for the training and testing process of the network. The testing data is not shown to the system until the testing stage of the network in order to reach realistic results via the proposed models.

ANFIS has been used in this paper to predict the next step force based on the history of the sample extension. There is a need for a sequencing block in the estimation of tensile as there is a dependency on the past values of standard extension.

2.ANFIS-based Prediction Model of Tool-Chip Contact Length

Being a Takagi–Sugeno type artificial intelligence model which is used to solve nonlinear and complicated problems, ANFIS is a hybrid system comprised of an artificial neural network and a fuzzy inference system (FIS). This implies that ANFIS is capable of self-learning and reasoning operation. ANFIS's fuzzy rules are as below:

Rule 1: if t is O_1, and x is P_1 then $z_1 = a_1 t + a_2 x + a_3$.

Rule 2: if t is O_2, and x is P_2 then $z_2 = b_1 t + b_2 x + b_3$.

In Rules 1 and 2, the variables t and x are inputs. The outputs z_1 and z_2 are specified by Rules 1 and 2. The parameters a_1, a_2, a_3, b_1, b_2, and b_3 are acquired during the learning process. As seen in Fig. 6, the ANFIS structure comprises five levels, each with one output and two inputs. Each layer has the following meaning: The first layer is a layer of fuzzification that employs the membership functions in computing fuzzy clusters according to the training input data. The indexes ai and bi are utilized to establish the membership function and calculate the membership's degree as:

$$Q_i^1 = \mu_{A_i}(x) = \frac{1}{1 + \left|\frac{x - c}{a}\right|^{2b}};\ i = 1,2 \tag{3}$$

$$Q_i^1 = \mu_{B_i}(x);\ i = 1,2 \tag{4}$$

in which membership degrees are μ_x and μ_y. Fuzzy sets are A_i and B_i. x and Q_i^1 are the input and the i^{th} node in the j^{th} layer output.

The rule is layer 2, which is utilized to double the firing power. The output should be calculated as:

$$Q_i^2 = w_i = \mu_{A_i}(x).\mu_{B_i}(y), i = 1,2 \tag{5}$$

Layer 3 is for normalizing the prior layer's firing intensity. The normalized values are generated by dividing the i^{th} rule's firing strength by the summation of all firing strengths:

$$Q_i^3 = \overline{w}_i = \frac{w_i}{w_1 + w_2 + w_3 + w_4}, i = 1, \cdots, 4 \tag{6}$$

Layer 4 is the layer of defuzzification. The result is computed as the normalized firing strength and the parameter set dot product (p_i, q_i and r_i) as:

$$Q_i^4 = \overline{w}_i f_i = \overline{w}_i (p_i x + q_i y + r_i) \tag{7}$$

The final result of Layer 5 is created by adding the defuzzification outputs of each rule:

$$Q_i^5 = \sum_i \overline{w}_i f_i = \frac{\sum_i w_i f_i}{\sum_i w_i} \tag{8}$$

The error signals from the output to the input layers are computed using the gradient descent approach's backpropagation algorithm. By adjusting the customizable parameters, the algorithm attempts to minimize the training error.

3.GA-based Hyperparameters Tunning

The GA belongs to the group of evolutionary-based algorithms, which is based on the evolutionary algorithms' natural selection. Mitchell [42] devised this approach according to the natural selection process. Genetic algorithms often start with generating a randomly produced population of chromosomes. Following that, the created chromosomes are "assessed" using an objective function, and those that best approximate the "ideal solution" to the issue have a higher probability of reproducing. In the present investigation, the population size is 80. The small population size imposes a constraint on the GA search capabilities. Additionally, the large population increases optimization length without significantly improving the outcomes. The GA results reveal that the mutation parameter, the crossover parameter, the generation parameter, and the population parameter has been all selected appropriately in this investigation.

4.PSO-based Hyperparameters Tunning

Kennedy *et al.* [43] developed PSO as a swarm-based algorithm category of the meta-heuristic algorithms. PSO is a stochastic population-based optimization method performed via the collaborative behaviour of a different colony of species known as populations [44]. It is similar to evolutionary computation methods such as GA [42]. It starts by defining the initial particles to evaluate the objective function at every particle's

location. It then decides the minor objective function as the best location. It calculates the new velocities according to the best position of the practices and their neighbours and the current velocity. The mentioned procedure continues iteratively until the algorithm fulfils the stopping criteria. PSO is capable of improving the candidate solution of an optimization problem, iteratively [45].

5.GWO-based Hyperparameters Tunning

Mirjalili *et al.* [46] created the Gray wolf optimization (GWO) method, which requires fewer parameters to be specified than a particle swarm optimization or genetic algorithm. It is simple to tune controller settings, maintaining a balance between exploration and exploitation. GWO mimics grey wolves' social behaviour. A pack of grey wolves is divided into four distinct groups: alphas, betas, deltas, and omegas. All other solutions are omegas, and all these agents must guide them. Qazani *et al.* [47] used GWO in motion cueing algorithm to extract the optimal weights of model predictive control. A cost (fitness) function is required for GWO to calculate the proposed techniques' ideal hyperparameters.

6.Bayesian-based Hyperparameters Tunning

Having been introduced by Thomas Bayes, the Bayes theory is usually used to extract the probability of the incident using the knowledge of the system in statistics [38]. A Bayesian optimization method is a bounded solver to calculate the states of the system in order to minimize the cost function [48]. The cost function can be stochastic or deterministic. Also, the state can be integers, continuous reals, or categorical. The Bayesian optimization method is used in the deep learning method for automatic tuning of the network. It should be noted that the acquisition functions modify their anticipated location of the state based on the proposed method by Gelbart, Snoek, and Adams [49]. The Bayesian optimization method is used to extract the hyperparameter of the ANFIS.

7.Cost Function

The three evolutionary-based optimization methods, including GA, PSO and GWO, as well as the global-based optimization method (Bayesian optimization), are tried to extract the optimal solution of the system

best on the user-defined objective function. After establishing the architecture of ANFIS, it is necessary to obtain the model's hyperparameters using optimization methods. The objective function should be defined properly to fulfil the requirement of the system. As an application for the prediction of the tool-chip contact length, the cost function is defined based on the MSE and CC between the actual and predicted tool-chip contact length during the testing process of the algorithms as follows:

$$J = \overbrace{\frac{1}{n}\sum_{i=1}^{n}\left(T_i - \hat{T}_i\right)^2}^{\text{MSE}} + \overbrace{\left(1 - \frac{\sum_{i=1}^{n}(x_i - \bar{x})\,(T_i - \bar{T})}{\sqrt{\sum_{i=1}^{n}(x_i - \bar{x})^2\,(T_i - \bar{T})^2}}\right)}^{\text{CC}} \tag{9}$$

where n, x_i and $\bar{x}$ are the number of test samples, the i^{th} input and mean of inputs, respectively. Also, T_i, $\bar{T}$, and $\hat{T}_i$ are the i^{th} output, mean of outputs and the i^{th} predicted value.

In Eq. (23), the first and second terms of the formula are defined based on the MSE and CC between the actual and predicted tool-chip contact length during the testing process of the samples. It should be noted that as the perfect prediction model yields to CC=1, then the CC term is subtracted from 1 inside the formula.

IV. Results and Discussions

Five models have been investigated in this study to estimate the tool–chip contact length using cutting speed, feed-rate and depth of cut. The previously developed GP model by Zadshakoyan and Pourmostaghimi [19] is used to show the significance of this study compared to others. Then, the five investigated models are GP (previously developed model [19]), GA-ANFIS (optimal ANFIS using a genetic algorithm), PSO-ANFIS (optimal ANFIS using particle swarm optimization), GWO-ANFIS (optimal ANFIS using grey wolf optimization) and B-ANFIS(optimal ANFIS using Bayesian optimization method). They are modelled in MATLAB. This Section consists of two subsections regarding the verification and validation of this study.

1.Verification

The considered models in Section III with four optimization methods are developed in MATLAB. ANFIS is proposed according to the described model in Section III.2. Then, the model is optimized based on the four optimization methods in Sections III.3-6. The cost function is defined in Section III.7, which is used inside the optimizer to extract the penalty value of the process.

The ANFIS function of MATLAB is used to design the ANFIS model. The proposed algorithms in Section III are developed under the MATLAB coding environment, and all the results are extracted using the plot function. In addition, the GA, PSO and Bayesian optimization methods are developed using the ga, particleswarm and bayesopt function of MATLAB. Also, GWO is employed via the provided code in FileExchange [50].

Four optimization methods are used to extract the optimal hyperparameters of the proposed ANFIS. Table 2 shows the optimized hyperparameters of the proposed ANFIS utilized for the prediction of the tool-chip contact length dataset.

The fitness function of these optimization processes for four models, including GA-ANFIS, PSO-ANFIS, GWO-ANFIS and B-ANFIS, are reported in Fig. 7a-d, respectively. Fig. 7a presents the fitness function of the GA-ANFIS regarding the five prementioned hyperparameters (membership function, epoch number, initial step size, step size decrease rate and step size increase rate). Also, Fig. 7b presents the fitness function for extraction of the optimal hyperparameters of the PSO-ANFIS. After developing these five investigated models in MATLAB software, they have been compared to show the efficiency of PSO-ANFIS in predicting too-chip contact length with better accuracy and minimum error. Moreover, Fig. 7c-d shows the convergence of fitness function using GWO and Bayesian methods. The extracted fuzzy membership functions and rules using the GWO method are a candidate to be presented in this study based on three inputs (speed, feed-rate and depth of cut) and one output (tool-chip contact length) for a better explanation of the proposed method.

Fig. 8a-c shows the membership functions of three inputs, including normalized cutting speed, feed-rate and depth of cut using GWO-ANFIS, respectively. The Gaussian membership function is employed in this study

to reach a fast and smooth response. Based on the represented results in Table 2 and Fig. 8, two membership functions for each input are optimized, and hyperparameters of the ANFIS are extracted by all optimization methods.

Also, Fig. 9a-c shows the extracted fuzzy rule surface based on the couple arrangement of inputs and output. Fig. 9a shows the variation of output (contact length) based on the variation of feed-rate and depth of cut. It should be noted that the parameters, including inputs and output, are normalized in Fig 8-9. Fig. 9b shows the variation of output based on the variation of cutting speed and depth of cut. Finally, Fig. 9c represents the variation of contact length based on the variation of speed and feed-rate. Based on the represented results in Fig. 9a-c, the depth of cut has a minor impact on the tool-chip contact length. Based on the represented results in Fig. 9a, feed-rate has more effect on the tool-chip contact length rather than the depth of cut. It also shows that the higher feed-rate and depth of cut result from the higher tool-chip contact length. In addition, the influence of the velocity is more than the depth of cut based on the represented results in Fig. 9b. Following the same behaviour of the feed-rate, the higher velocity results in the higher toll-chip contact length. Finally, Fig. 9c shows that the influence of the velocity in the variation of tool-chip contact length is more than the feed-rate. In the next subsection, the extracted and developed models are tested and validated in order to discover the most accurate model for the prediction of the contact length based on the input cutting parameters.

2.Validation

Table 3 represents the results during the training and testing processes of the investigated methods. Based on the represented results, GP is the weakest method in the point of MSE, root means square error (RMSE), and normalized root means square error (NRMSE) compared with the other four optimized ANFIS models during the testing process. Also, in point of CC and R2, B-ANFIS is the weakest method in comparison with the other three optimized ANFIS models as well as the GP model. The lowest MSE and RMSE during the testing is achieved via GWO-ANFIS with 235.7567 and 15.3544, respectively. In addition, the lowest MSE and RMSE during the training are achieved via B-ANFIS with 10.8040 and 15.3544, respectively. The highest

CC and R2 during the training are reached via B-ANFIS with 0.4884 and 0.4973, respectively. Also, the best CC and R2 of testing are 0.9648 and 0.9286 via GWO-ANFIS, respectively. The most accurate prediction during training and testing of each sample are bolded in Table 3 to discover the accurate proposed method.

The graphical representation of Table 3 is shown in Fig. 10a-b, which tries to show the experimental and predicted tool-chip contact length during the training and testing, respectively. 36 datasets are selected for training (80%), and 8 are chosen for the testing purpose of the developed methods (20%). Based on the represented results in Fig. 10a, it is obvious that B-ANFIS can predict the results more accurate than the other investigated models, including GP, GA-ANFIS, PSO-ANFIS and GWO-ANFIS, during the training process of the algorithms. However, the results during the testing process of the investigated method are important in choosing the most accurate model. Based on the represented results in Fig. 10b, the predicted tool-chip contact length via GWO-ANFIS (black times signs) is the closest value to the actual tool-chip contact length (red cross sign) recorded via the experimental setup during the testing process. Also, the B-ANFIS has an overshooting problem during the testing process, as it is shown in samples 4 and 8 of Fig. 10b. It makes B-ANFIS unreliable for the prediction of tool-chip contact length, while it can reach very accurate results during the training process of the model.

Fig. 11a-e shows the error using five developed methods, including GP, GA-ANFIS, PSO-ANFIS, GWO-ANFIS and B-ANFIS, during the training and testing process of the networks. It should be noted that the red colour plot is used to show the error of networks during the training process. Also, the blue colour plot shows the error of the networks during the testing process. Based on the represented results in Fig. 11a-e, the highest and lowest RMSE between the actual and predicted tool-chip contact length during the testing process using 5 investigated methods are via GP and GWO-ANFIS with 3010 and 236 (μm), respectively. In addition, the RMSE between the actual and predicted too-chip contact length during testing for GP, GA-ANFIS, PSO-ANFIS, GWO-ANFIS and B-ANFIS are 54.85, 16.71, 15.64, 15.35 and 47.96 (μm), respectively.

Fig. 12a-e represents the error histogram of the predicted data during the training and testing process of the methods, including GP, GA-ANFIS, PSO-ANFIS, GWO-ANFIS and B-ANFIS, respectively. Fig. 12a shows

that the error histogram of the GP has a normal distribution with a higher range of error which is between -100 to 100 (μm). In addition, PSO-ANFIS has a normal distribution of error in the range of -30 to 30 (μm). The error histogram of GA-ANFIS has left-skewed based on the represented results in Fig. 12b. The average error between the actual and predicted too-chip contact length using GP, GA-ANFIS, PSO-ANFIS, GWO-ANFIS and B-ANFIS are -1.0346, 2.3469, 1.8823, 2.1830 and 24.7547 (μm), respectively.

The regression plot of the developed four methods, including GA-ANFIS, PSO-ANFIS, GWO-ANFIS and B-ANFI for all data (including training and testing), are shown in Fig. 12a-d, respectively. The R2 of GA-ANFIS, PSO-ANFIS, GWO-ANFIS and B-ANFI during training and testing are 0.62647, 0.63473, 0.63124 and 0.64895, respectively.

Finally, Table 4 represents the mathematical values of all represented Figs in this Section for a better understanding of the investigated methods and a fair comparison between them. It includes MSE, RMSE, NRMSE, an average of error, variation of error, CC and R2 of the five investigated methods, including GA-ANFIS, PSO-ANFIS, GWO-ANFIS, B-ANFIS and GP.

It should be noted that the higher efficiency of the ANFIS model in handling the complex dataset in the existence of the limited number of data is the main motivation for this paper, which leads to higher prediction power compared to the previously proposed method using GP [51-54]. The represented results in this Section prove the efficiency of proposed novel optimized ANFIS models compared with previous artificial intelligent prediction methods (GP) in terms of higher CC and R2 as well as lower MSE, RMSE and NRMSE. In addition, the GWO-ANFIS can reach better results in comparison with the other three optimized methods, including GA-ANFIS, PSO-ANFIS and B-ANFIS. Also, B-ANFIS was able to defeat the other optimized algorithm in the majority of samples. However, some overshoot in testing data decreases the efficiency of this model dramatically.

V. CONCLUSION

Tool-chip contact length is one of the essential parameters in metal cutting as it can affect the cutting pressures, tool wear, tool life, cutting temperatures, and chip formation. The reduction of tool-chip contact length reduces the shear zone temperature and cutting force. Based on the following facts, it is important to estimate the tool-chip contact length based on the cutting parameters, including depth of cut, feed-rate, and cutting speed. This study presents a new ANFIS model to estimate the tool-chip contact length in orthogonal cutting. The evolutionary and global-based optimization techniques extract the optimal hyperparameters of models. Also, one of the previous prediction models, genetic programming, is designed and validated to prove the efficiency of the proposed method. The investigated models are tested using the cutting parameters and tool-chip contact length plots. The prediction accuracy of the proposed models is determined by using different parameters, including CC, MSE, RMSE, NRMSE, and R-square. The five investigated methods are modelled in MATLAB software using MATLAB functions, and then the results are extracted based on the division of data for 90% training and 10% testing. The extracted results prove that GWO-ANFIS can reach better results during the training and testing compared to those of previous GP, GA-ANFIS, PSO-ANFIS, and B-ANFIS. In addition, the recalculated fuzzy logic rule surface during the training process of the ANFIS model shows that the tool-chip contact length directly relates to cutting speed, feed-rate, and depth of cut. Also, the cutting speed and depth of cut have the most and least effective in the variation of the tool-chip contact length during the orthogonal cutting process. In future work, an ensemble method with different accurate neural network models can be utilized to increase the accuracy of the predicted values of tool-chip contact length. As a future study, other types of evolutionary-based optimization, such as social group optimization algorithm [55-58], and another advanced form of neural network model [59-65], can be used for extracting the cutting parameters reaching minimum tool-chip contact length.

Conflicts of Interest: The authors declare that they have no conflicts of interest to report regarding the present study.

REFERENCES

1. Poletika, M., *Contact loads on tool faces (Russian)*, in *Machinostronie, Moscow*. 1969.
2. Friedman, M. and E. Lenz, *Investigation of the tool-chip contact length in metal cutting.* International Journal of Machine Tool Design and Research, 1970. **10**(4): p. 401-416.
3. Kato, S., K. Yamaguchi, and M. Yamada, *Stress distribution at the interface between tool and chip in machining.* 1972.
4. Sadik, M.I. and B. Lindström, *The role of tool-chip contact length in metal cutting.* Journal of Materials Processing Technology, 1993. **37**(1-4): p. 613-627.
5. Sadik, M.I. and B. Lindström, *The effect of restricted contact length on tool performance.* Journal of Materials Processing Technology, 1995. **48**(1-4): p. 275-282.
6. Abukhshim, N., P. Mativenga, and M. Sheikh, *An investigation of the tool-chip contact length and wear in high-speed turning of EN19 steel.* Proceedings of the Institution of Mechanical Engineers, Part B: Journal of Engineering Manufacture, 2004. **218**(8): p. 889-903.
7. Sutter, G., *Chip geometries during high-speed machining for orthogonal cutting conditions.* International Journal of Machine Tools and Manufacture, 2005. **45**(6): p. 719-726.
8. Korkut, I. and M. Donertas, *The influence of feed rate and cutting speed on the cutting forces, surface roughness and tool–chip contact length during face milling.* Materials & design, 2007. **28**(1): p. 308-312.
9. Iqbal, S., P. Mativenga, and M. Sheikh, *A comparative study of the tool–chip contact length in turning of two engineering alloys for a wide range of cutting speeds.* The International Journal of Advanced Manufacturing Technology, 2009. **42**(1): p. 30-40.
10. Devillez, A., S. Lesko, and W. Mozer, *Cutting tool crater wear measurement with white light interferometry.* Wear, 2004. **256**(1-2): p. 56-65.
11. Mikolajczyk, T. *Modeling of minimal thickness cutting layer influence on surface roughness in turning*. in *Applied Mechanics and Materials*. 2014. Trans Tech Publ.
12. Mohapatra, S., H. Sarangi, and U. Mohanty, *Analysis of Chip–Tool Contact Length for Developed Centrifugal Cutting Tool and Conventional High-Speed Cutting Tool Using Predictive Models*, in *Current Advances in Mechanical Engineering*. 2021, Springer. p. 779-788.
13. Ortiz-de-Zarate, G., et al., *A novel methodology to characterize tool-chip contact in metal cutting using partially restricted contact length tools.* CIRP Annals, 2021. **70**(1): p. 61-64.
14. Zhang, L., et al., *Modeling and analysis of tool-chip contact model during quasi-intermittent vibration assisted swing cutting based on two-zone theory.* The International Journal of Advanced Manufacturing Technology, 2022: p. 1-12.
15. Suvarna, M., et al., *Smart manufacturing for smart cities—overview, insights, and future directions.* Advanced Intelligent Systems, 2020. **2**(10): p. 2000043.
16. Sheptunov, S.A., et al. *Simulation of Thermoset Heat Conductivity by Means of Artificial Neural Networks*. in *2018 IEEE International Conference" Quality Management, Transport and Information Security, Information Technologies"(IT&QM&IS)*. 2018. IEEE.
17. Durodola, J., *Machine learning for design, phase transformation and mechanical properties of alloys.* Progress in Materials Science, 2022. **123**: p. 100797.
18. Ostad-Ali-Askari, K., M. Shayannejad, and H. Ghorbanizadee-Kharazi, *Assessment of artificial neural network performance and exponential regression in prediction of effective rainfall.* International Journal of Development Research, 2015. **5**(3): p. 3791-3794.
19. Zadshakoyan, M. and V. Pourmostaghimi, *Genetic equation for the prediction of tool–chip contact length in orthogonal cutting.* Engineering Applications of Artificial Intelligence, 2013. **26**(7): p. 1725-1730.
20. Zadshakoyan, M. and V. Pourmostaghimi, *Metaheuristics in manufacturing: predictive modeling of tool wear in machining using genetic programming*, in *Advancements in applied metaheuristic computing*. 2018, IGI Global. p. 118-142.
21. Pourmostaghimi, V. and M. Zadshakoyan, *Optimization of cutting parameters during hard turning using evolutionary algorithms.* Optimization for Engineering Problems, 2019: p. 77-99.
22. Nguyen-Le, D.H., et al., *A data-driven approach based on long short-term memory and hidden Markov model for crack propagation prediction.* Engineering Fracture Mechanics, 2020. **235**: p. 107085.
23. Xu, L.-H., et al., *Prediction of cutting power and surface quality, and optimization of cutting parameters using new inference system in high-speed milling process.* Advances in Manufacturing, 2021. **9**(3): p. 388-402.
24. Qazani, M.R.C., et al. *A Novel Motion Control Mechanism for Satellite Tracking Antenna Using Fuzzy Logic Control of Serial Robot*. in *2021 IEEE International Conference on Systems, Man, and Cybernetics (SMC)*. 2021. IEEE.
25. Qazani, M.R.C., H. Asadi, and S. Nahavandi, *A new gantry-tau-based mechanism using spherical wrist and model predictive control-based motion cueing algorithm.* Robotica, 2020. **38**(8): p. 1359-1380.
26. Qazani, M.R.C., et al., *Adaptive Motion Cueing Algorithm Based on Fuzzy Logic Using Online Dexterity and Direction Monitoring.* IEEE Systems Journal, 2021.
27. Setia, S. and S.R. Chauhan, *An Improved Artificial Neural Networking Architecture Approach for Prediction of Cutting Parameters in Turning of EN31 Steel*, in *Optimization Methods in Engineering*. 2021, Springer. p. 377-401.
28. Charalampous, P., *Prediction of cutting forces in milling using machine learning algorithms and finite element analysis.* Journal of Materials Engineering and Performance, 2021. **30**(3): p. 2002-2013.
29. Annapurna, K. and A.m. Yesaswini, *Improved Hungarian Algorithm for Unbalanced Assignment Problems.* International Journal of communication and computer Technologies, 2021. **9**(1): p. 7.
30. Tran-Ngoc, H., et al., *Efficient Artificial neural networks based on a hybrid metaheuristic optimization algorithm for damage detection in laminated composite structures.* Composite Structures, 2021. **262**: p. 113339.
31. Wang, S., et al., *Automatic laser profile recognition and fast tracking for structured light measurement using deep learning and template matching.* Measurement, 2021. **169**: p. 108362.
32. Qazani, M.R.C., et al., *An optimal washout filter for motion platform using neural network and fuzzy logic.* Engineering Applications of Artificial Intelligence, 2022. **108**: p. 104564.
33. Qazani, M.R.C., H. Parvaz, and S. Pedrammehr, *Optimization of Fixture Locating Layout Design Using Comprehensive Optimised Machine Learning.* Research Square (Preprint), 2022: p. 1-40.
34. Zhang, Q., J. Sun, and E. Tsang, *An evolutionary algorithm with guided mutation for the maximum clique problem.* IEEE transactions on evolutionary computation, 2005. **9**(2): p. 192-200.
35. Banks, A., J. Vincent, and C. Anyakoha, *A review of particle swarm optimization. Part I: background and development.* Natural Computing, 2007. **6**(4): p. 467-484.
36. Wickramasinghe, K., *The Use of Deep Data Locality towards a Hadoop Performance Analysis Framework.* International Journal of communication and computer Technologies, 2020. **8**(1): p. 4.
37. Faris, H., et al., *Grey wolf optimizer: a review of recent variants and applications.* Neural computing and applications, 2018. **30**(2): p. 413-435.
38. Longenecker, R.N., *Paul, Apostle of Liberty*. 2015: Wm. B. Eerdmans Publishing.

39. Zadshakoyan, M. and V. Pourmostaghimi, *Cutting tool crater wear measurement in turning using chip geometry and genetic programming.* International Journal of Applied Metaheuristic Computing (IJAMC), 2015. **6**(1): p. 47-60.
40. Mikołajczyk, T., et al., *Influence of the main cutting edge angle value on minimum uncut chip thickness during turning of C45 steel.* Journal of Manufacturing Processes, 2020. **57**: p. 354-362.
41. Lee, E. and B. Shaffer, *The theory of plasticity applied to a problem of machining.* 1951.
42. Mitchell, M., *An introduction to genetic algorithms*. 1998: MIT press.
43. Kennedy, J. and R. Eberhart. *Particle swarm optimization (PSO)*. in *Proc. IEEE International Conference on Neural Networks, Perth, Australia*. 1995.
44. Zajmi, L., F.Y. Ahmed, and A.A. Jaharadak, *Concepts, methods, and performances of particle swarm optimization, backpropagation, and neural networks.* Applied Computational Intelligence and Soft Computing, 2018. **2018**.
45. Pourmostaghimi, V. and M. Zadshakoyan, *Designing and implementation of a novel online adaptive control with optimization technique in hard turning.* Proceedings of the Institution of Mechanical Engineers, Part I: Journal of Systems and Control Engineering, 2021. **235**(5): p. 652-663.
46. Mirjalili, S., S.M. Mirjalili, and A. Lewis, *Grey wolf optimizer.* Advances in engineering software, 2014. **69**: p. 46-61.
47. Qazani, M.R.C., et al. *An MPC-based Motion Cueing Algorithm Using Washout Speed and Grey Wolf Optimizer*. in *2021 IEEE International Conference on Systems, Man, and Cybernetics (SMC)*. 2021. IEEE.
48. Pelikan, M., D.E. Goldberg, and E. Cantú-Paz. *BOA: The Bayesian optimization algorithm*. in *Proceedings of the genetic and evolutionary computation conference GECCO-99*. 1999. Citeseer.
49. Gelbart, M.A., J. Snoek, and R.P. Adams, *Bayesian optimization with unknown constraints.* arXiv preprint arXiv:1403.5607, 2014.
50. Mirjalili, S. *Grey Wolf Optimizer (GWO)*. 2022 [cited February 8, 2022. February 8, 2022.]; Available from: https://www.mathworks.com/matlabcentral/fileexchange/44974-grey-wolf-optimizer-gwo.
51. Zhengcai, C., et al., *Bottleneck prediction method based on improved adaptive network-based fuzzy inference system (ANFIS) in semiconductor manufacturing system.* Chinese Journal of Chemical Engineering, 2012. **20**(6): p. 1081-1088.
52. Zhang, Y.-l. and J.-h. Lei, *Prediction of laser cutting roughness in intelligent manufacturing mode based on ANFIS.* Procedia engineering, 2017. **174**: p. 82-89.
53. Shabani, M.O., et al., *Performance of ANFIS coupled with PSO in manufacturing superior wear resistant aluminum matrix nano composites.* Transactions of the Indian Institute of Metals, 2018. **71**(9): p. 2095-2103.
54. Foorginejad, A., et al., *Modeling of weld bead geometry using adaptive neuro-fuzzy inference system (ANFIS) in additive manufacturing.* Journal of Applied and Computational Mechanics, 2020. **6**(1): p. 160-170.
55. Srinivasareddy, S., Y.V. Narayana, and D. Krishna, *Sector Beam Synthesis in Linear Antenna Arrays using Social Group Optimization Algorithm.* National Journal of Antennas and Propagation, 2021. **3**(2): p. 4.
56. Satapathy, S. and A. Naik, *Social group optimization (SGO): a new population evolutionary optimization technique.* Complex & Intelligent Systems, 2016. **2**(3): p. 173-203.
57. Naik, A. and S.C. Satapathy, *A comparative study of social group optimization with a few recent optimization algorithms.* Complex & Intelligent Systems, 2021. **7**(1): p. 249-295.
58. Kabir, H.D., et al., *Aleatory-aware deep uncertainty quantification for transfer learning.* Computers in Biology and Medicine, 2022: p. 105246.
59. Kumar, K., et al. *SpinalXNet: Transfer Learning with Modified Fully Connected Layer for X-Ray Image Classification*. in *2021 IEEE International Conference on Recent Advances in Systems Science and Engineering (RASSE)*. 2021. IEEE.
60. Qazani, M.R.C., et al. *A Fast and Reliable Approach for Driving Style Customization in Autonomous Vehicles*. in *2021 IEEE International Conference on Systems, Man, and Cybernetics (SMC)*. 2021. IEEE.
61. Qazani, M.R.C., et al., *Prediction of Motion Simulator Signals Using Time-Series Neural Networks.* IEEE Transactions on Aerospace and Electronic Systems, 2021.
62. Qazani, M.R.C., et al. *Time Series Prediction of Driving Motion Scenarios Using Fuzzy Neural Networks:* Motion Signal Prediction Using FNNs*. in *2021 IEEE International Conference on Mechatronics (ICM)*. 2021. IEEE.
63. Kabir, H.D., et al., *Neural Network Training for Uncertainty Quantification Over Time-Range.* IEEE Transactions on Emerging Topics in Computational Intelligence, 2020.
64. Kabir, H.D., et al., *Uncertainty-aware decisions in cloud computing: Foundations and future directions.* ACM Computing Surveys (CSUR), 2021. **54**(4): p. 1-30.
65. Adane, K. and B. Beyene, *Machine Learning and Deep Learning Based Phishing Websites Detection: The Current Gaps and Next Directions.* Review of Computer Engineering Research, 2022. **9**(1): p. 13-29.

Fig. 1. The orthogonal cutting process schematic presentation, the length of contact, actual chip thickness, undeformed chip thickness, and shear angle.

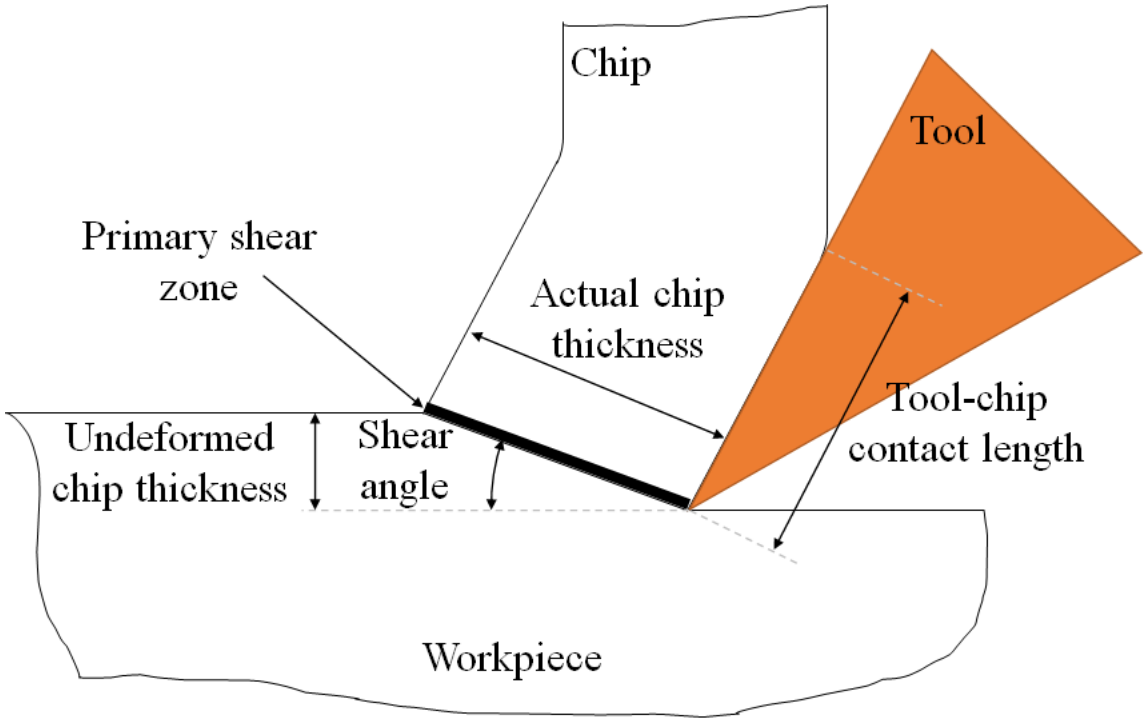


Fig. 2. Setup of the CNC lathe machine.

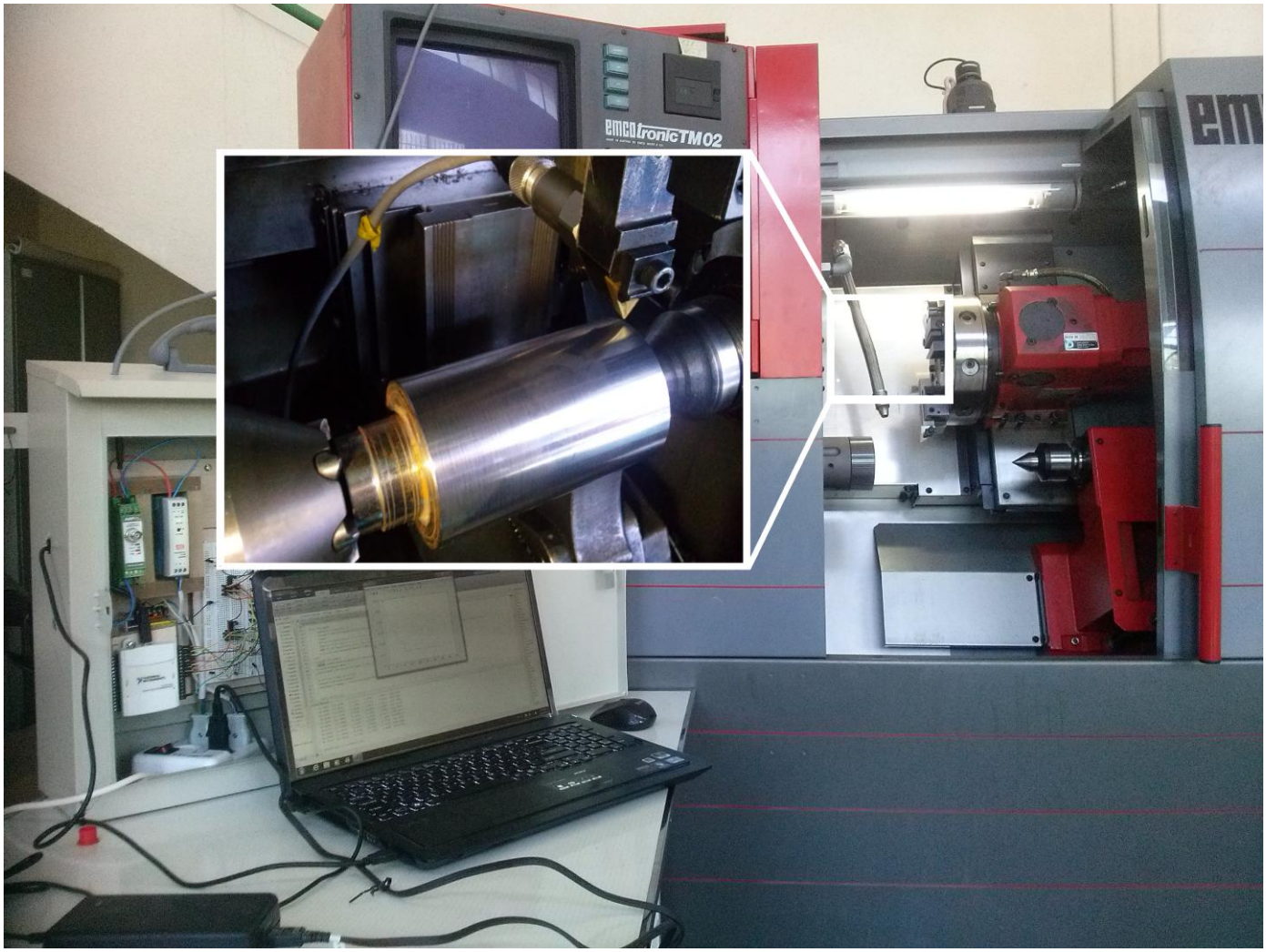


Fig. 3. Setup of the measurement process using the optical microscope equipped with image processing software.



Fig. 4. Optical microscopic images for tool-chip contact length for (a) v=55 m/min, f=0.2 mm/rev, a=2.7 mm and (b) v=107 m/min, f=0.06 mm/rev, a=1.8 mm.

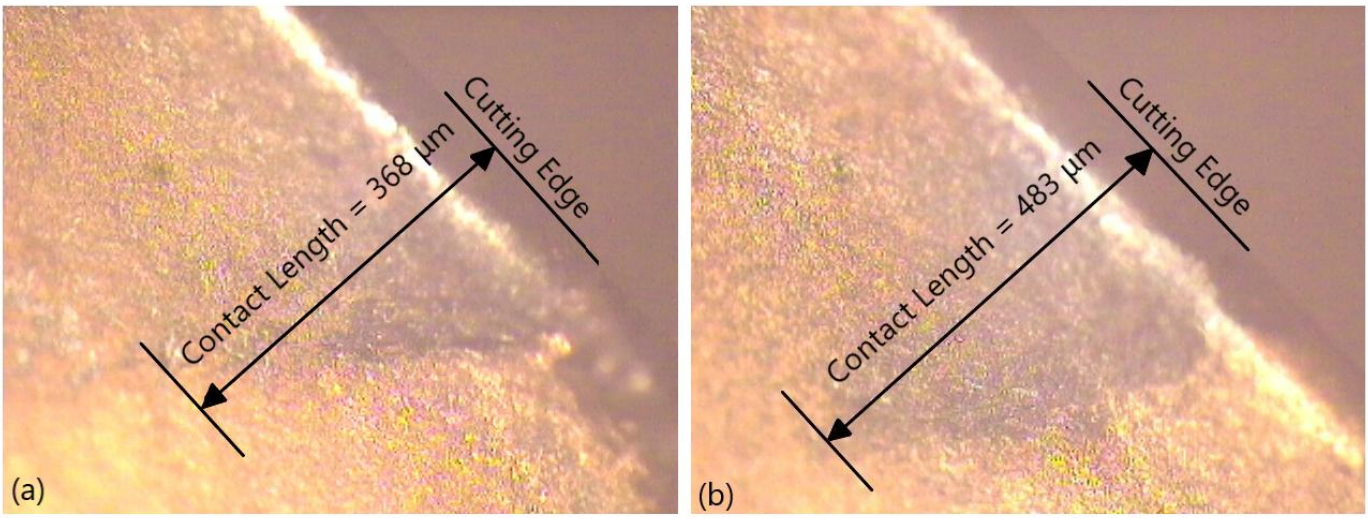
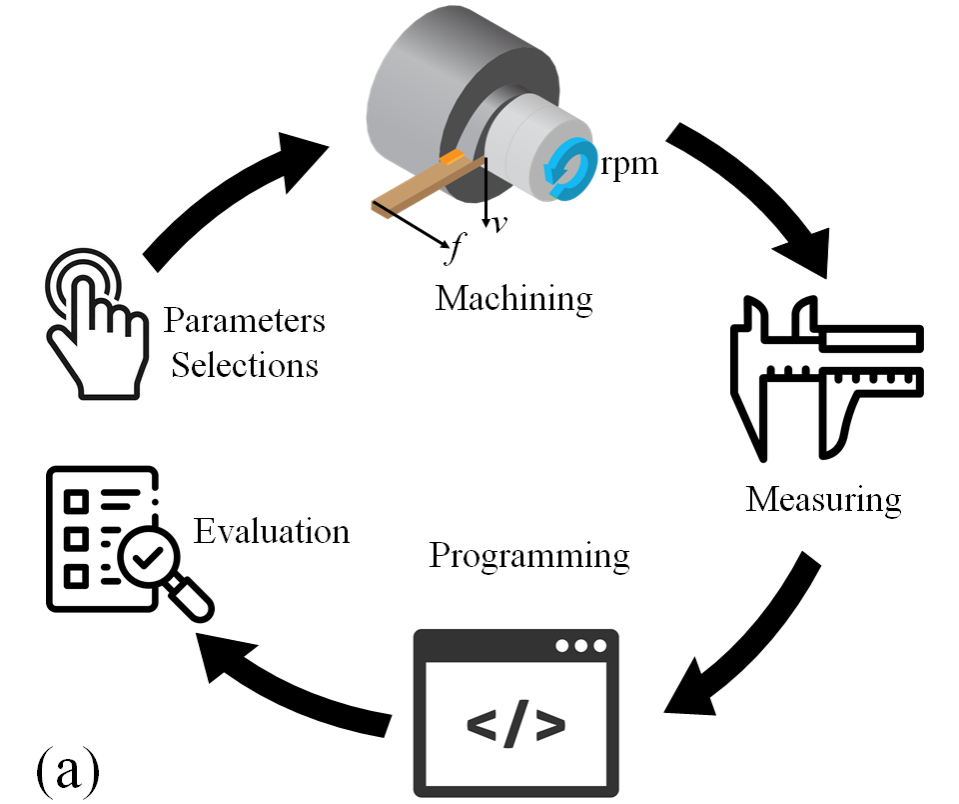


Fig. 5. The overview of the proposed method in this study for (a): the whole process; (b): the artificial intelligent part.



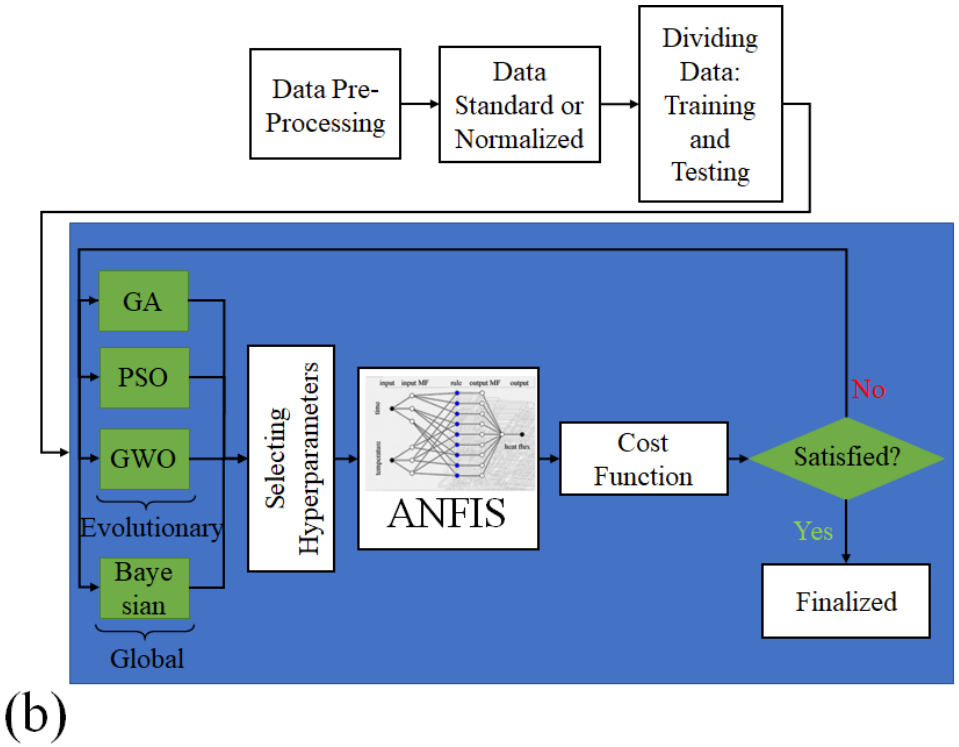


Fig. 6. The structure of ANFIS.

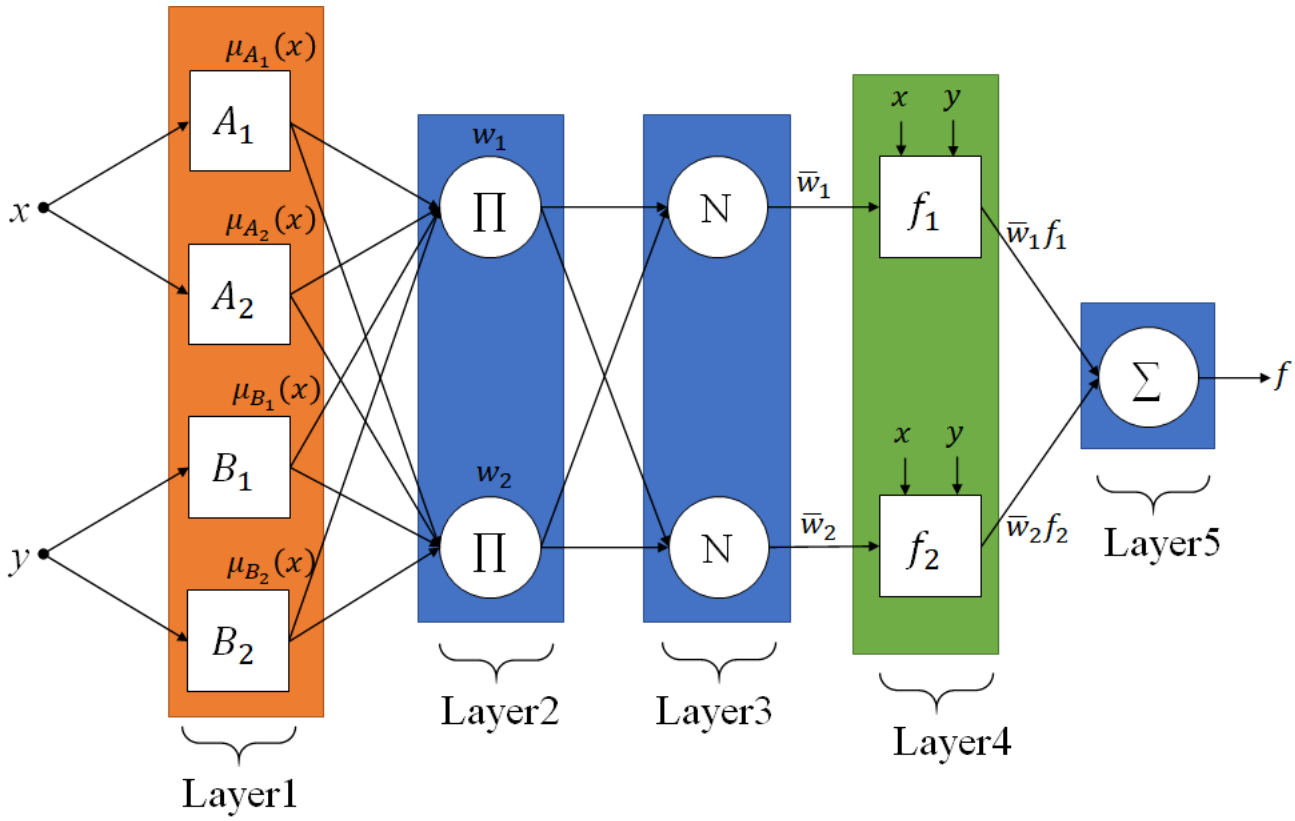
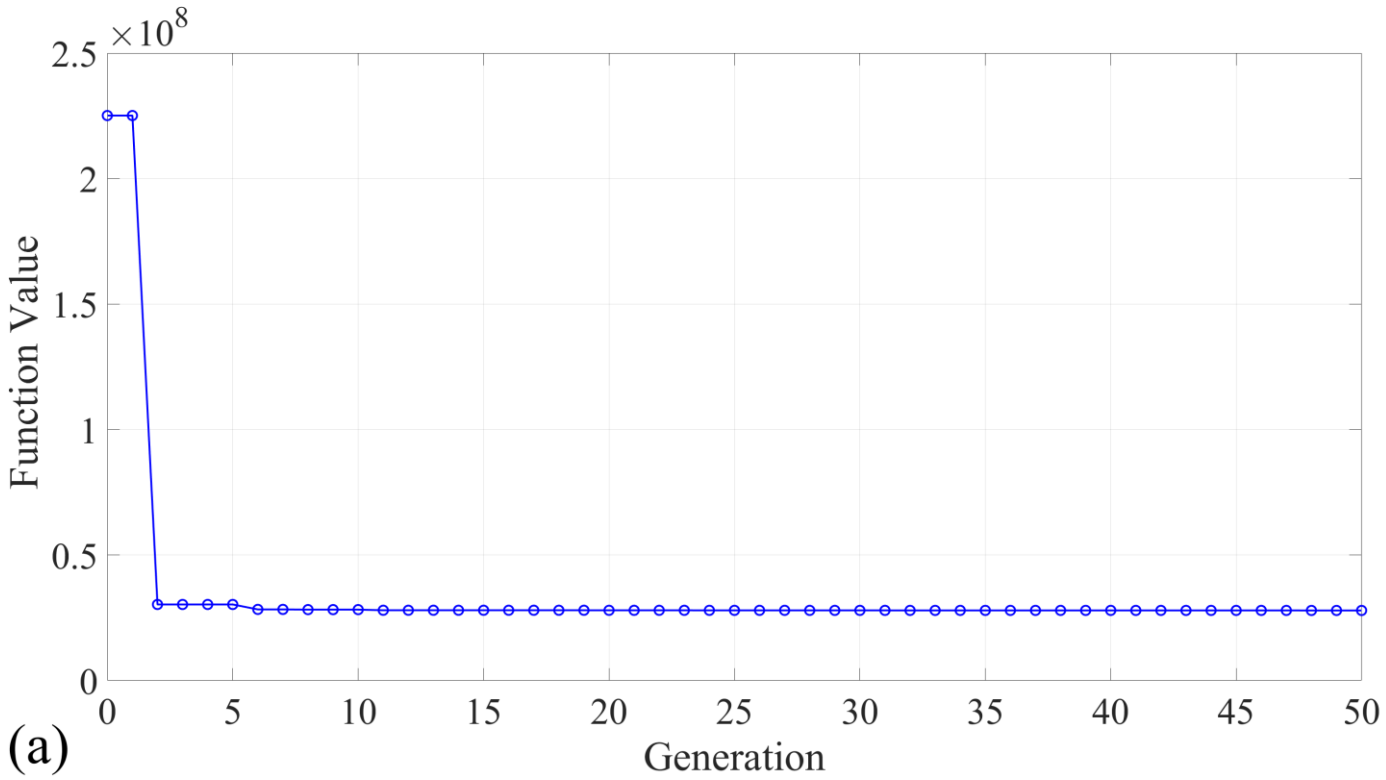
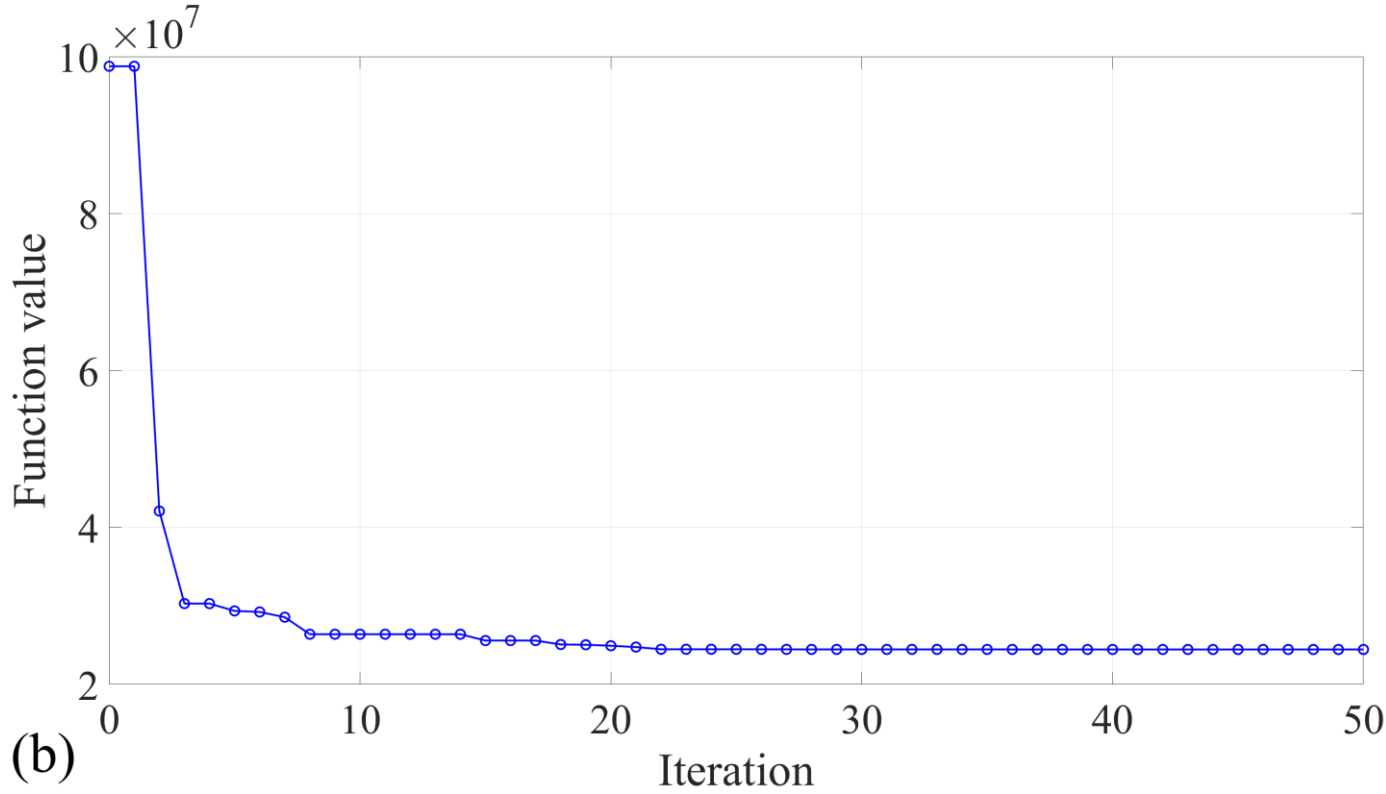


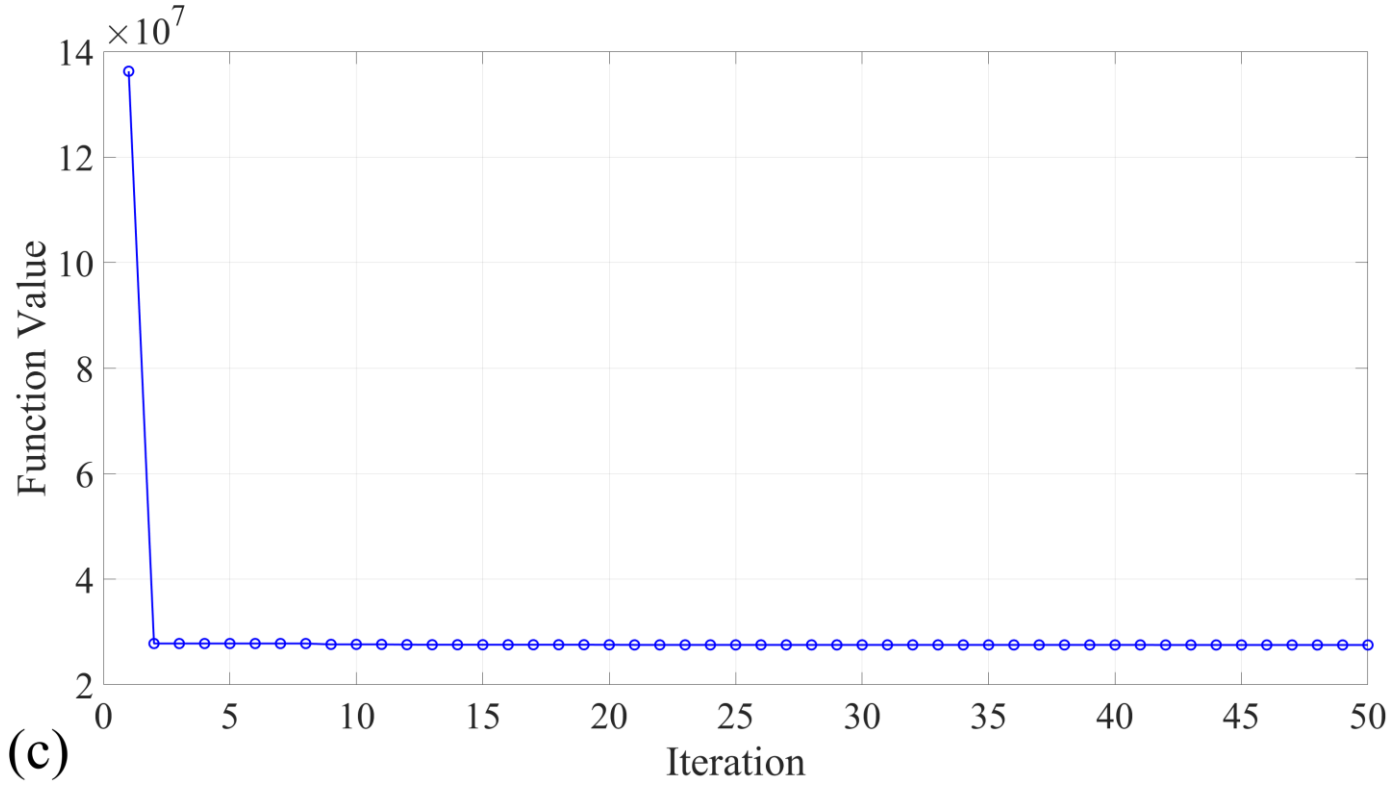
Fig. 7. The convergence of optimization methods including (a): GA; (b): PSO; (c): GWO; (d): Bayesian optimization.



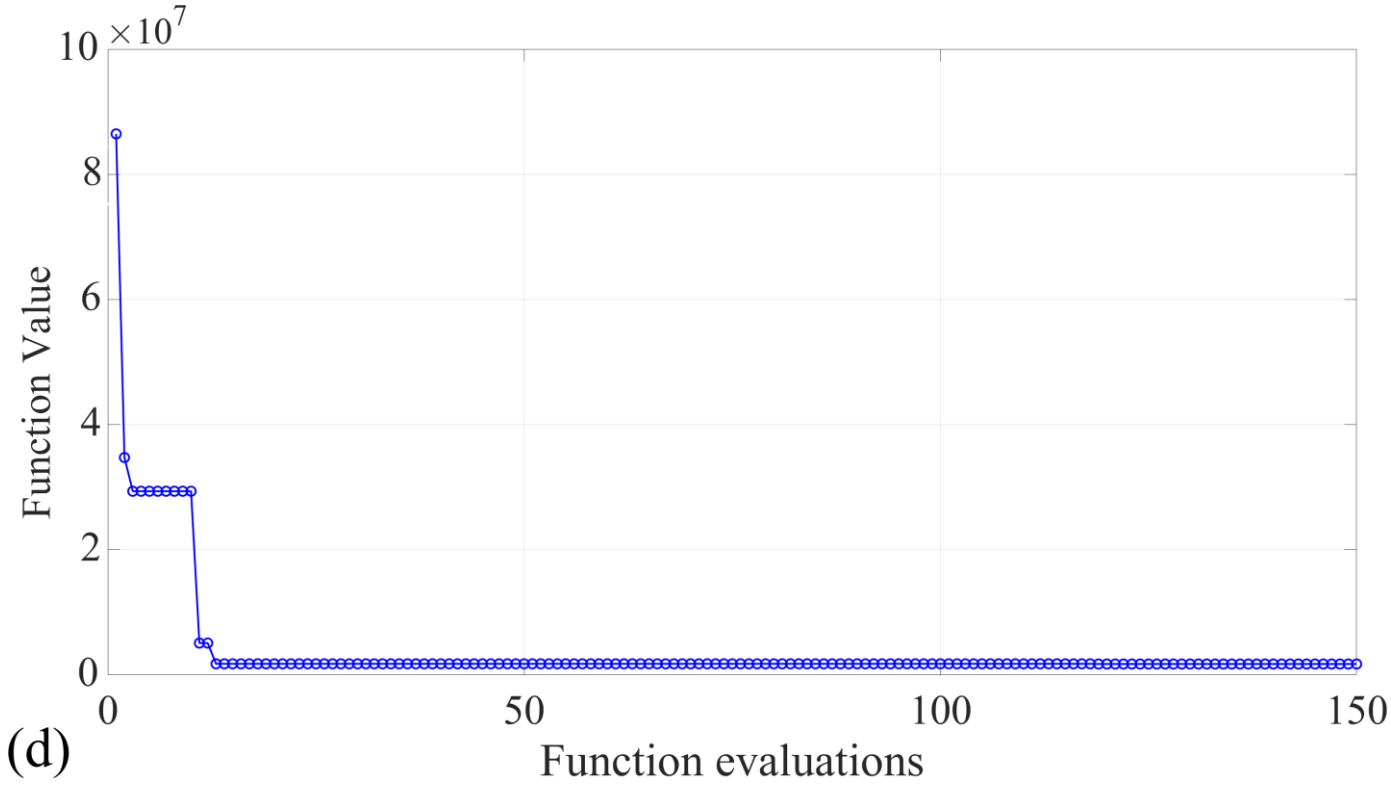
(a)



(b)


×10^7
14
12
10
8
6
4
2
Function Value
0
5
10
15
20
25
30
35
40
45
50
Iteration

(c)


×10^7
10
8
6
4
2
0
Function Value
0
50
100
150
Function evaluations

(d)

Fig. 8. The gaussian membership function of GWO-ANFIS for normalized inputs including (a): cutting speed; (b): feed-rate; (c): depth of cut.

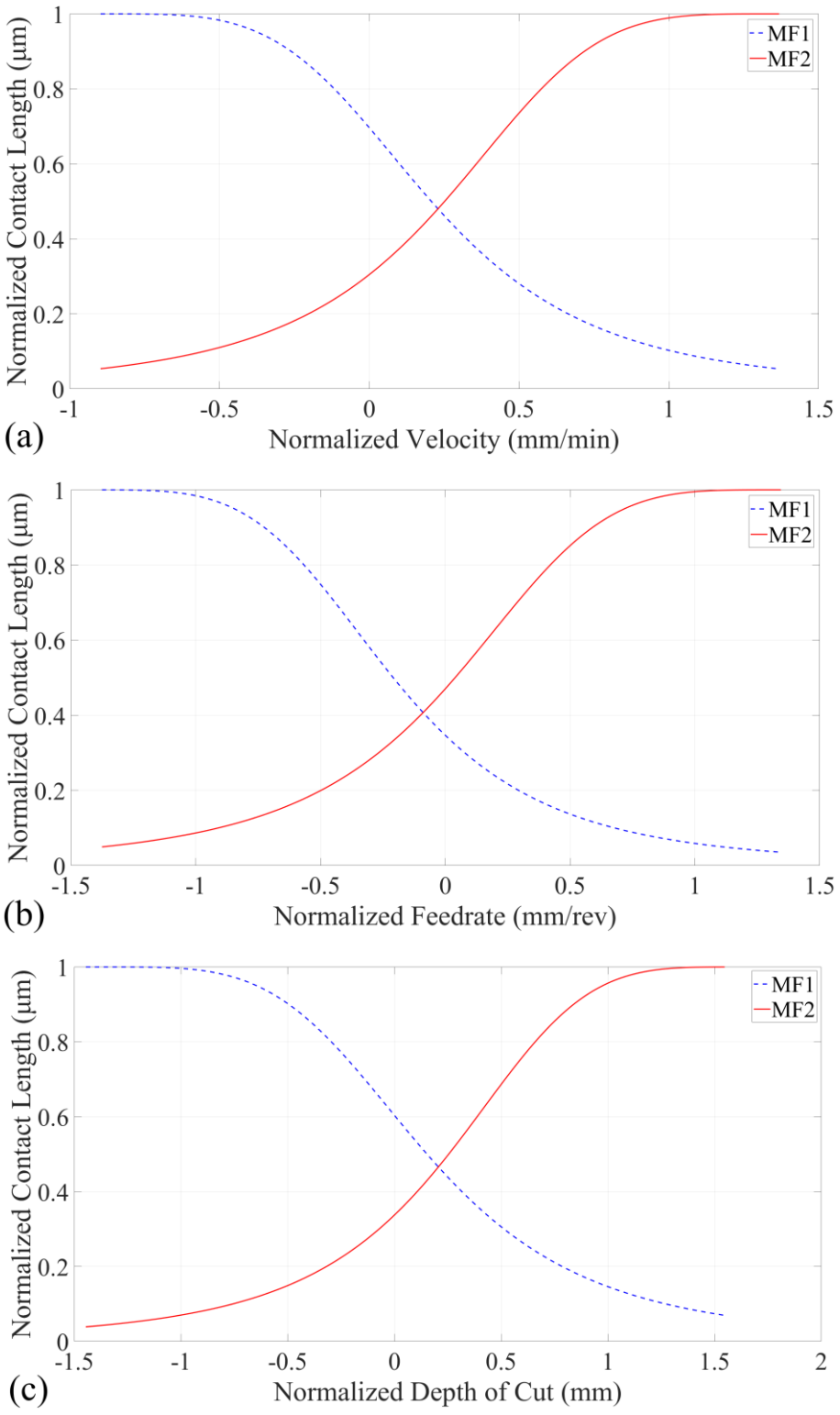
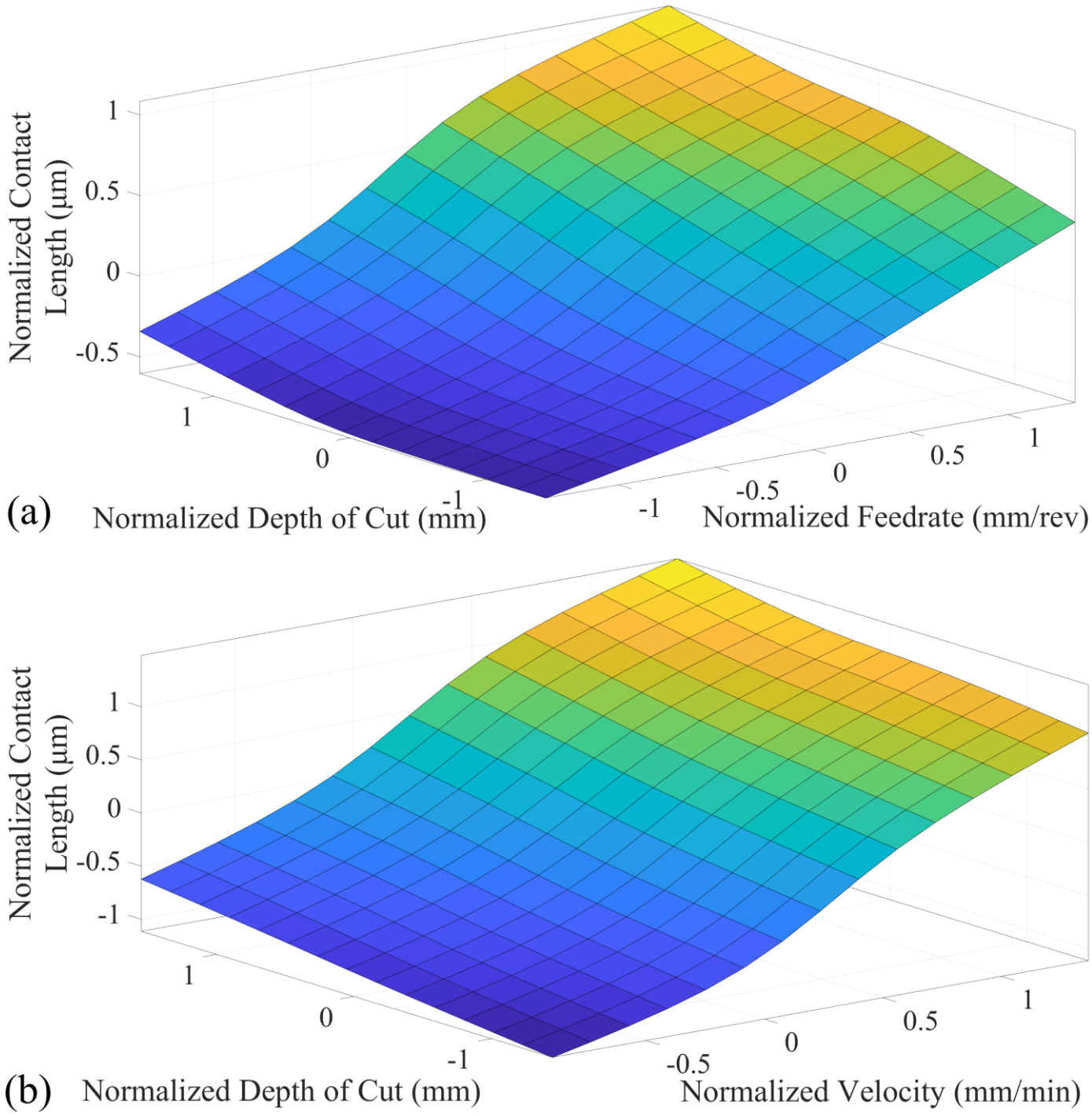
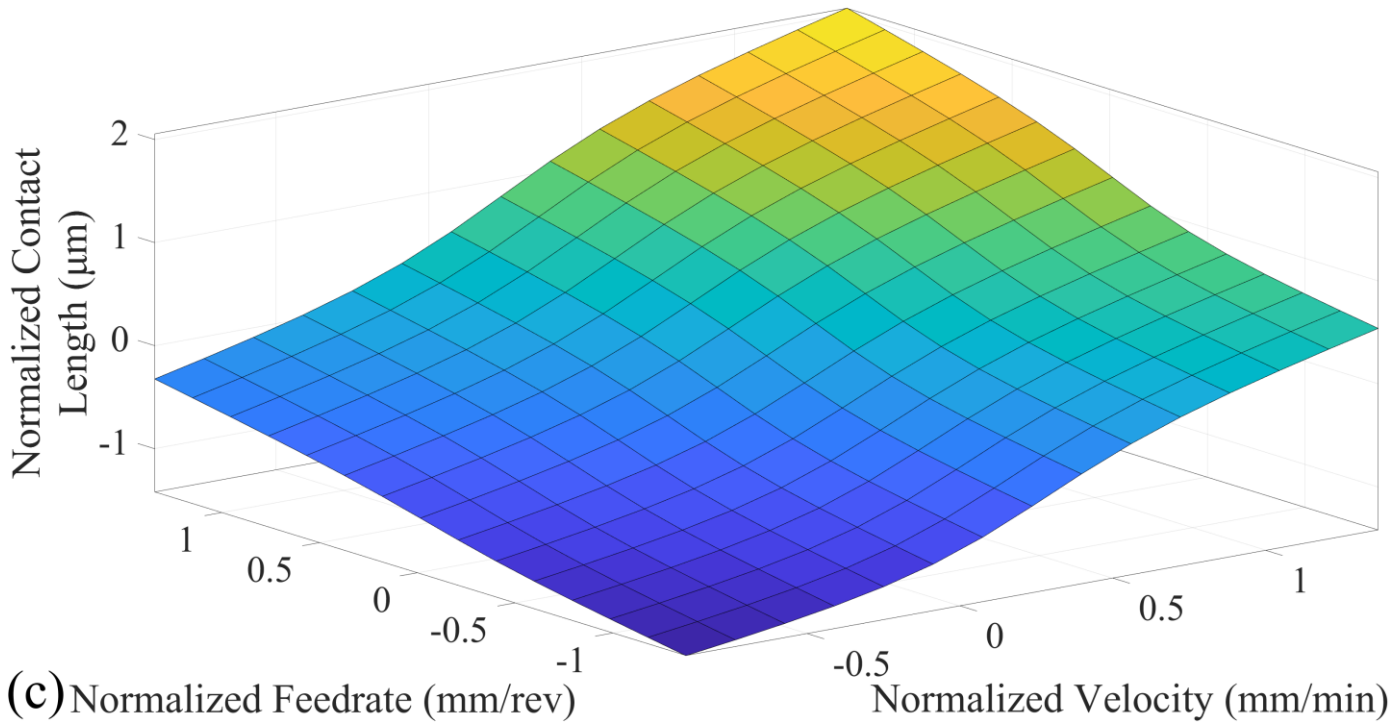


Fig. 9. The rule surface for GWO-ANFIS with variations of (a): feed-rate and depth; (b): speed and depth; (c): speed and feed-rate.




Normalized Contact Length (μm)
2
1
0
-1
1
0.5
0
-0.5
-1
Normalized Feedrate (mm/rev)
-0.5
0
0.5
1
Normalized Velocity (mm/min)

(c)

Fig. 10. The actual and predicted contact length using GP, GA-ANFIS, PSO-ANFIS, GWO-ANFIS and B-ANFIS for (a): training dataset; (b): testing dataset.

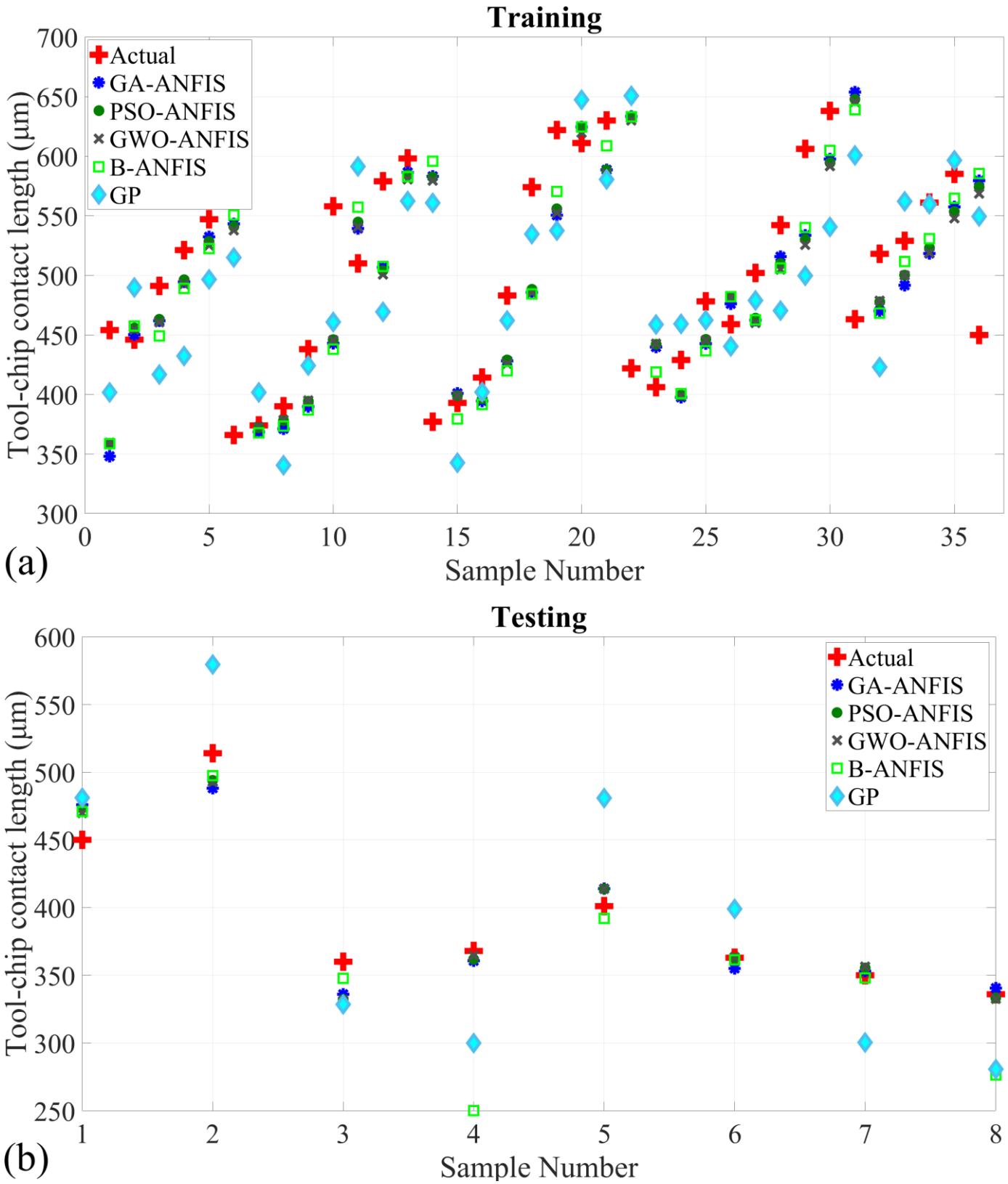
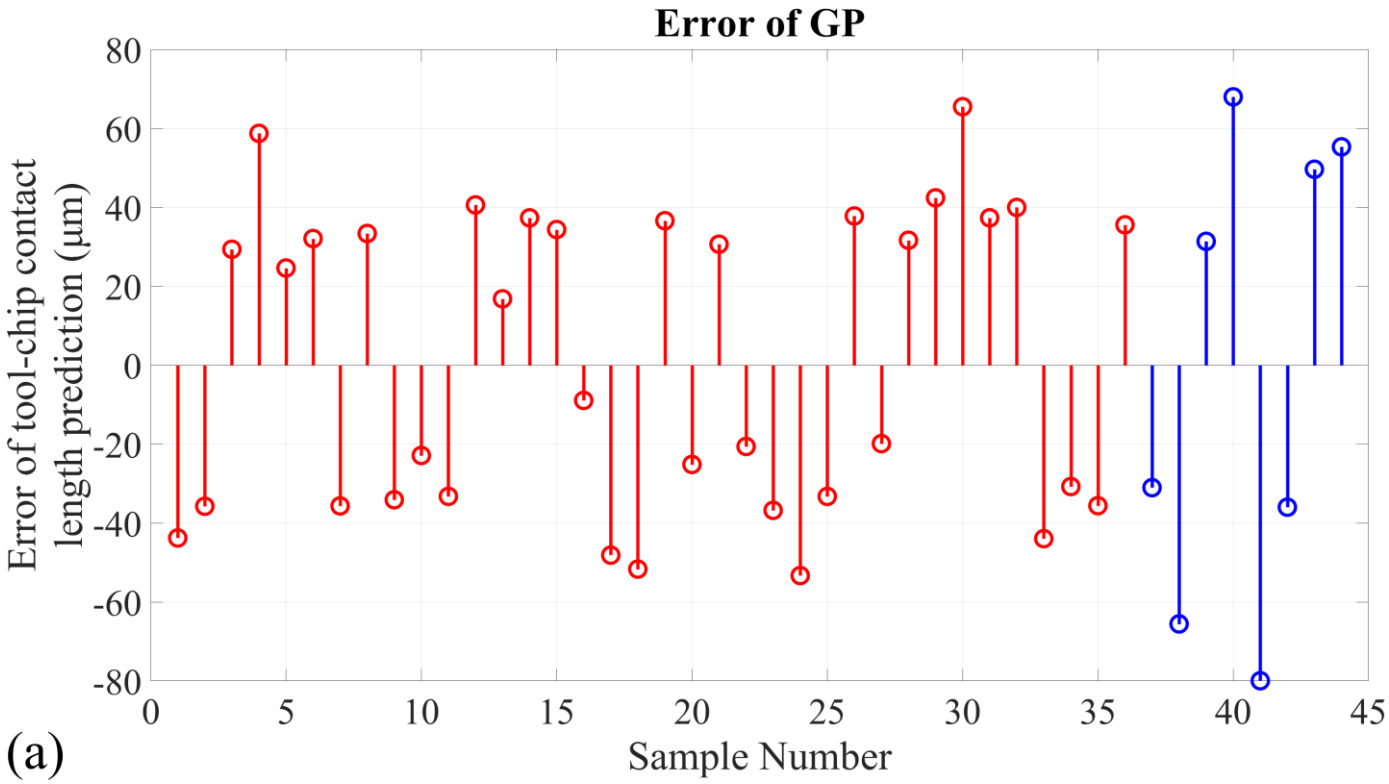
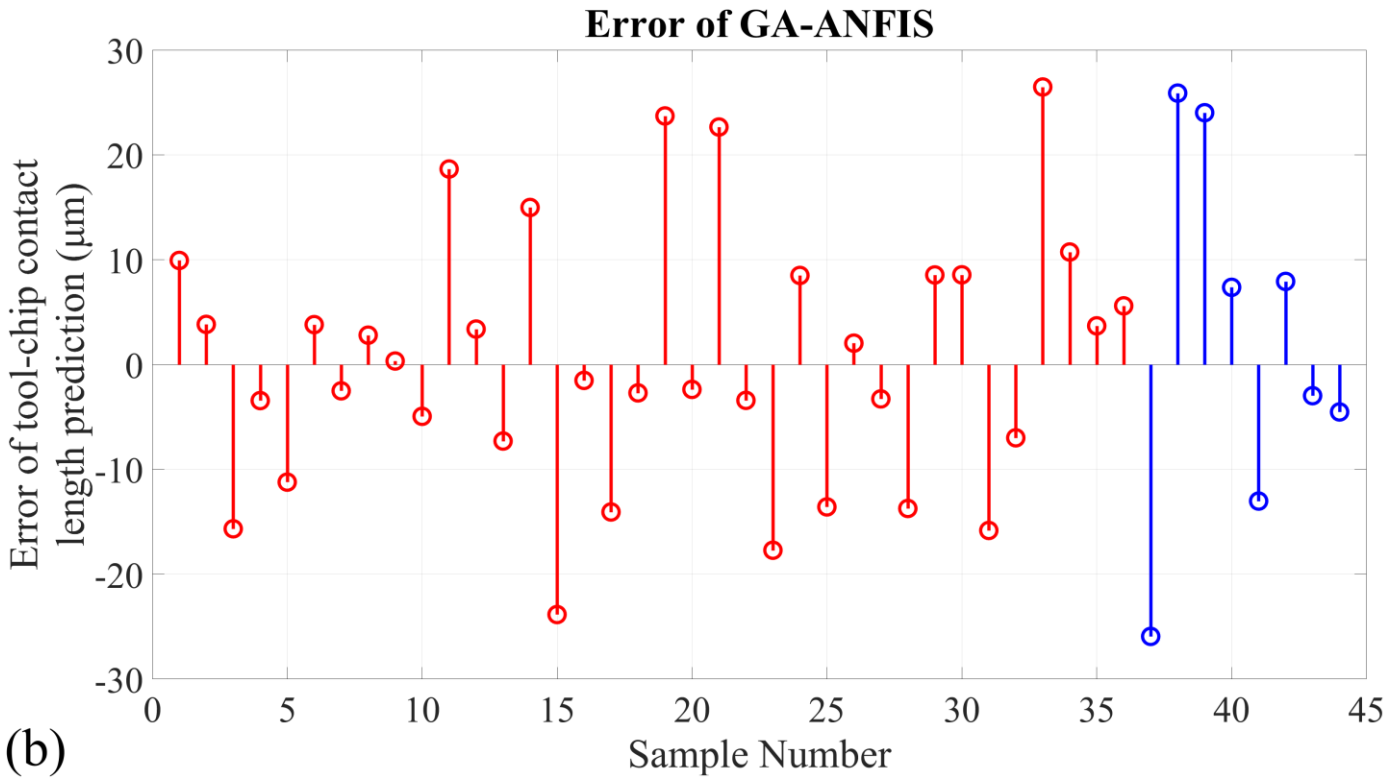


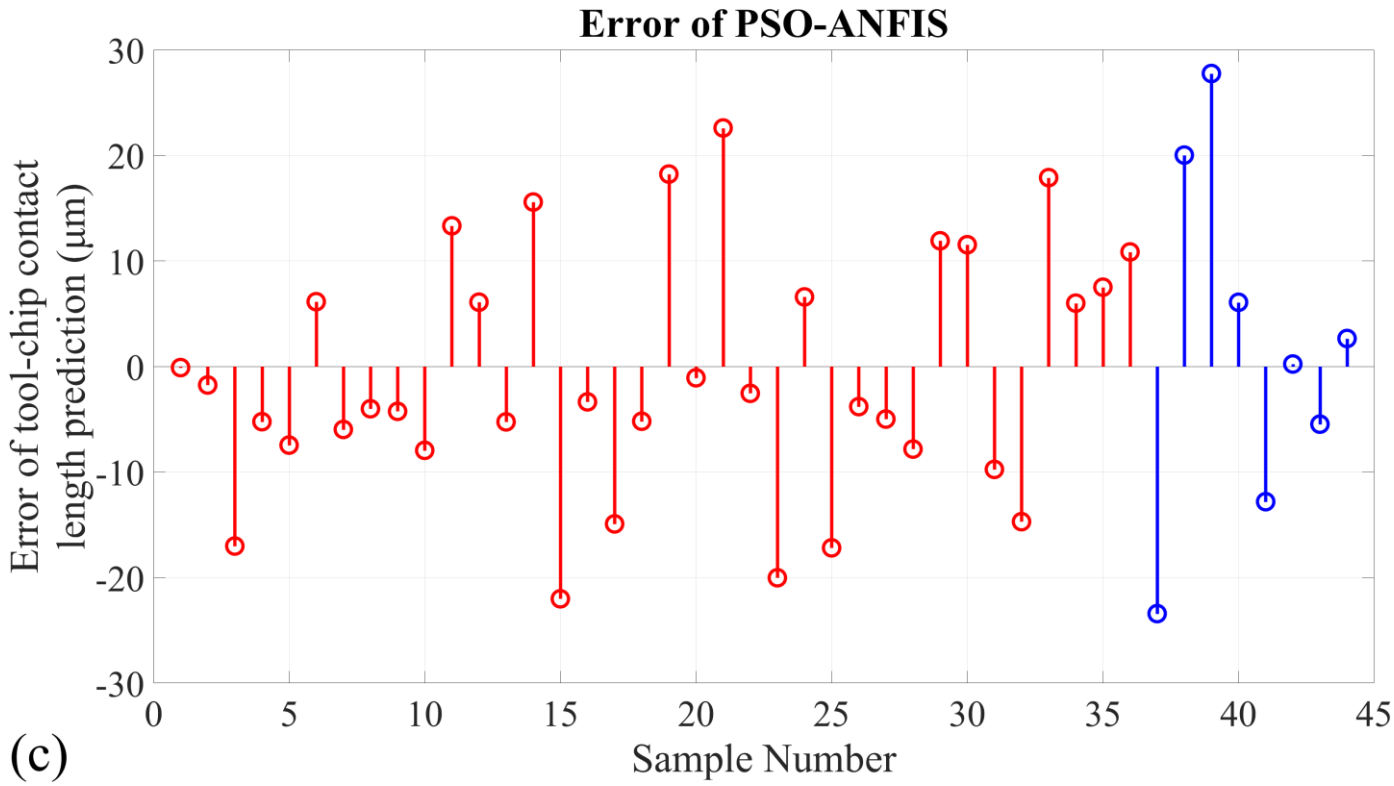
Fig. 11. The error between the actual and predicted tool-chip contact length for all data including training and testing using (a): GP; (b): GA-ANFIS; (c): PSO-ANFIS; (d): GWO-ANFIS; (e): B-ANFIS.



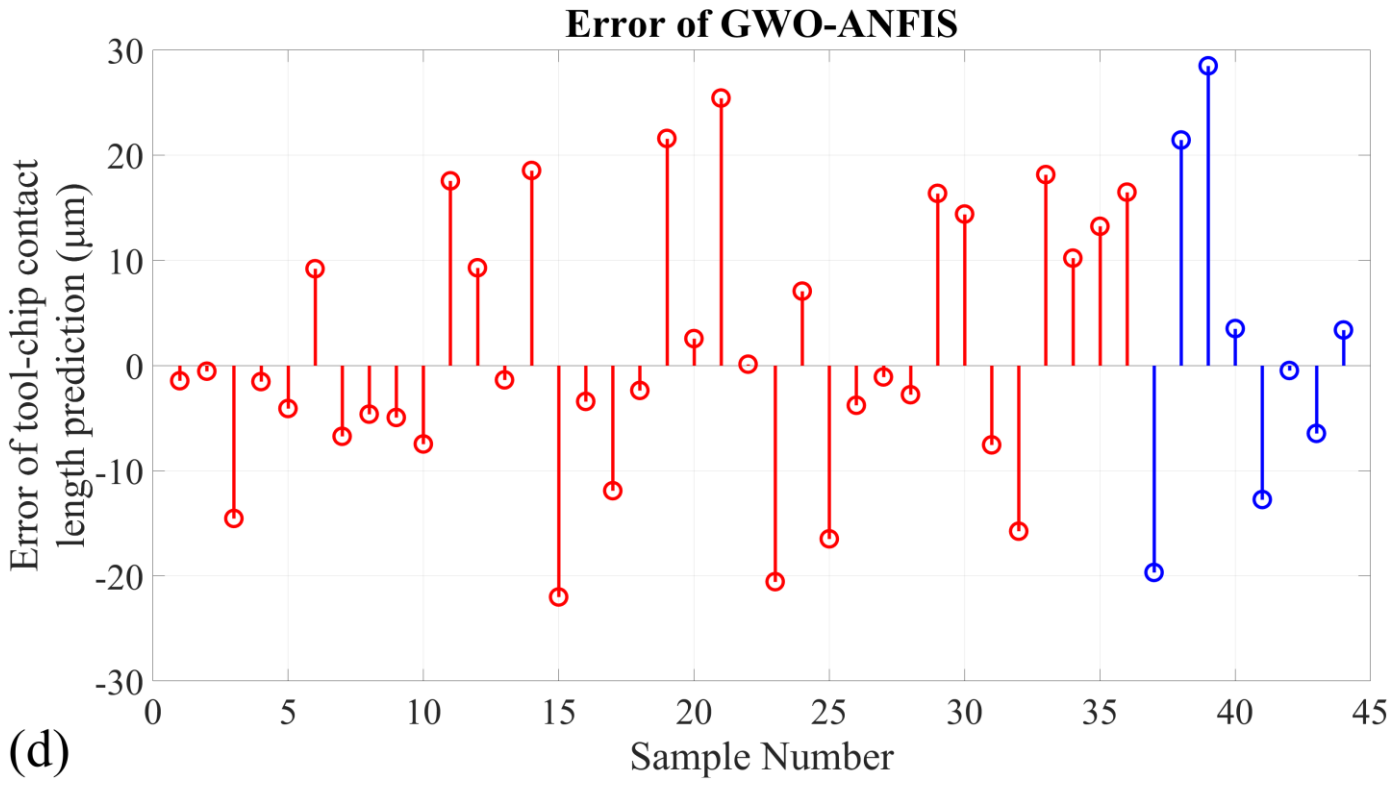
(a)



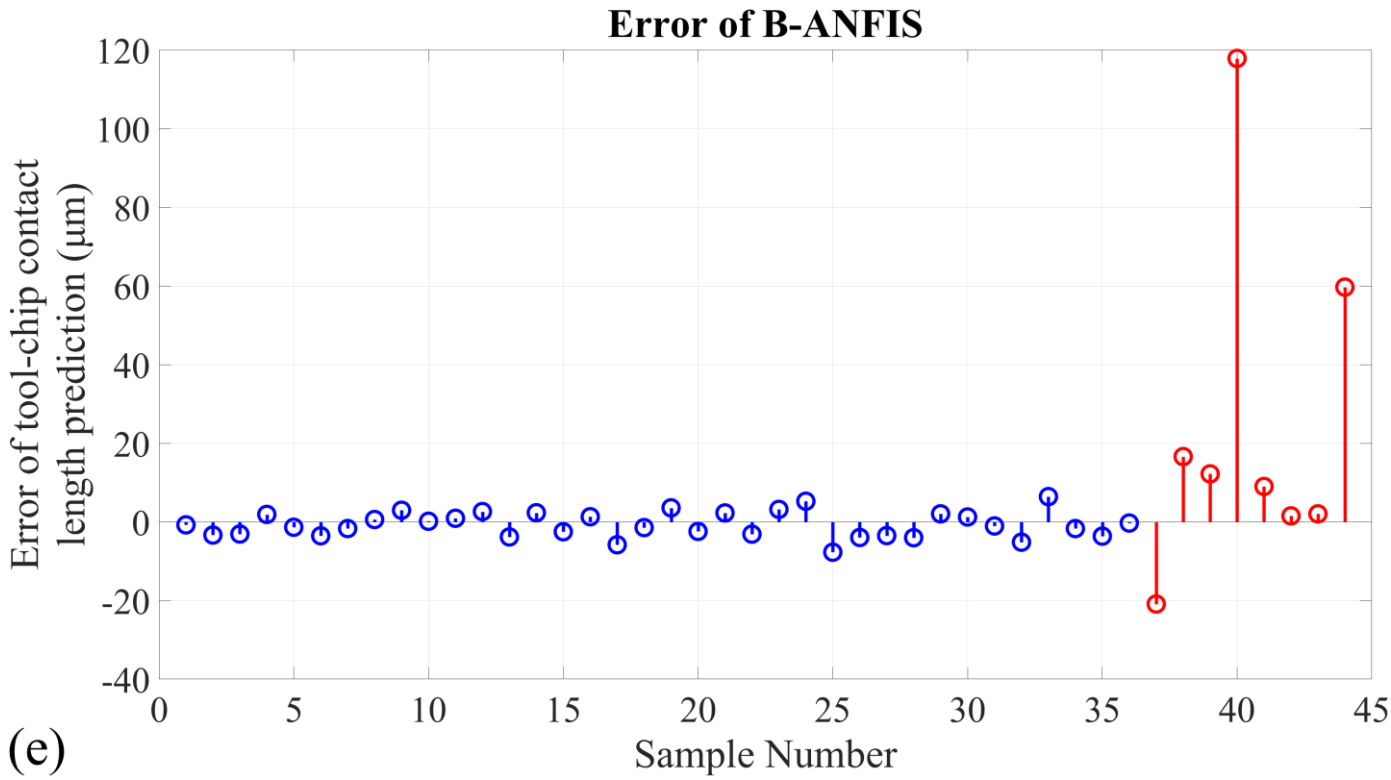
(b)


Error of PSO-ANFIS
Error of tool-chip contact length prediction (μm)
Sample Number
30
20
10
0
-10
-20
-30
0
5
10
15
20
25
30
35
40
45

(c)

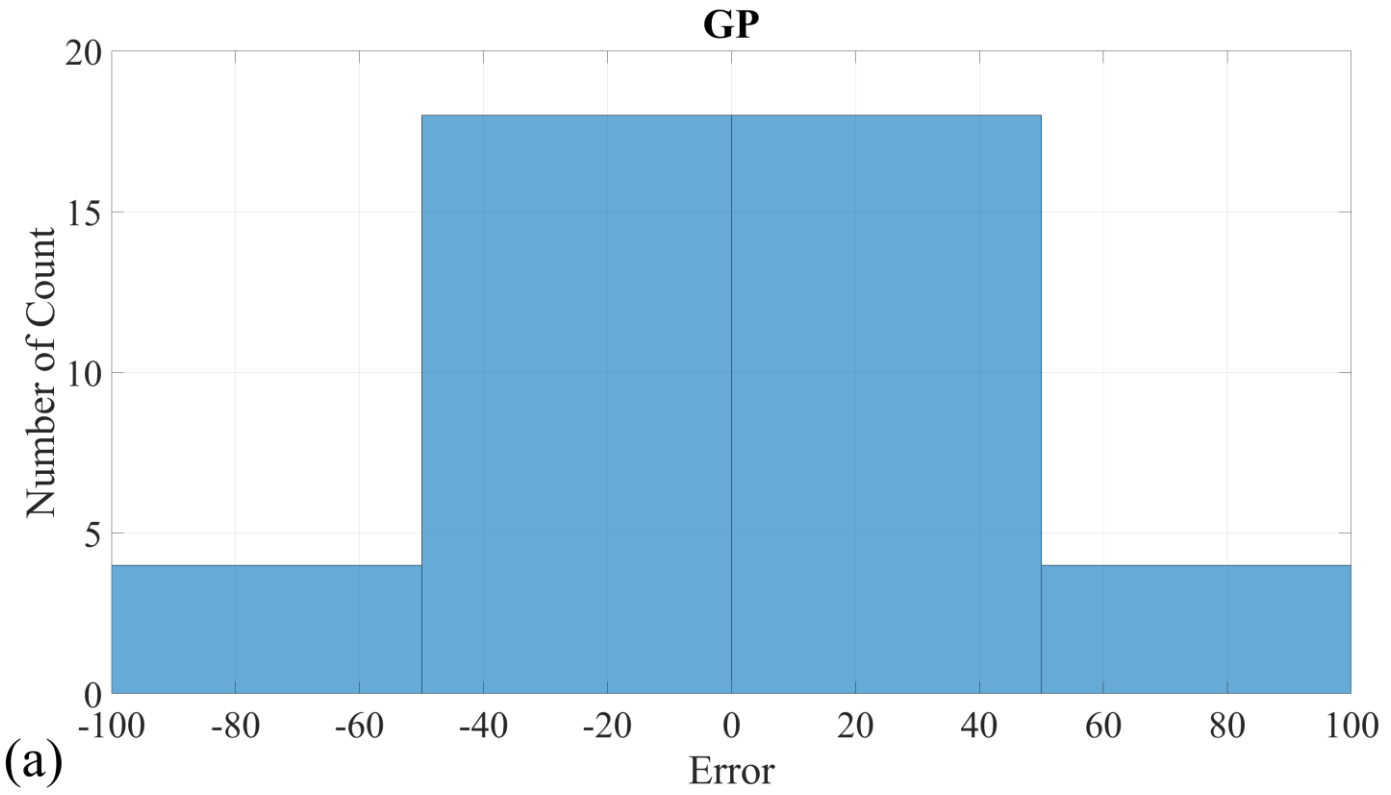

Error of GWO-ANFIS
Error of tool-chip contact length prediction (μm)
Sample Number
30
20
10
0
-10
-20
-30
0
5
10
15
20
25
30
35
40
45

(d)

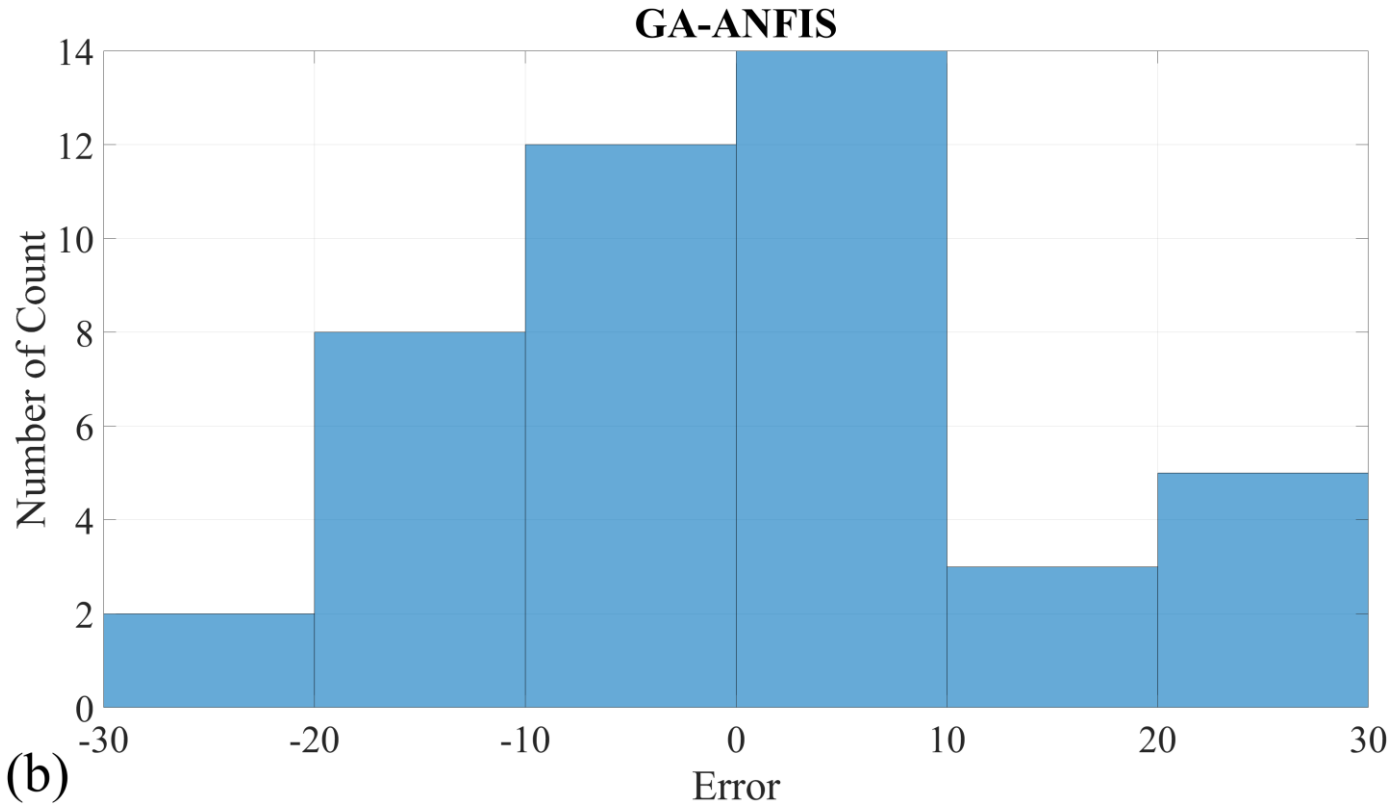

Error of B-ANFIS
Error of tool-chip contact length prediction (μm)
120
100
80
60
40
20
0
-20
-40
0
5
10
15
20
25
30
35
40
45
Sample Number

(e)

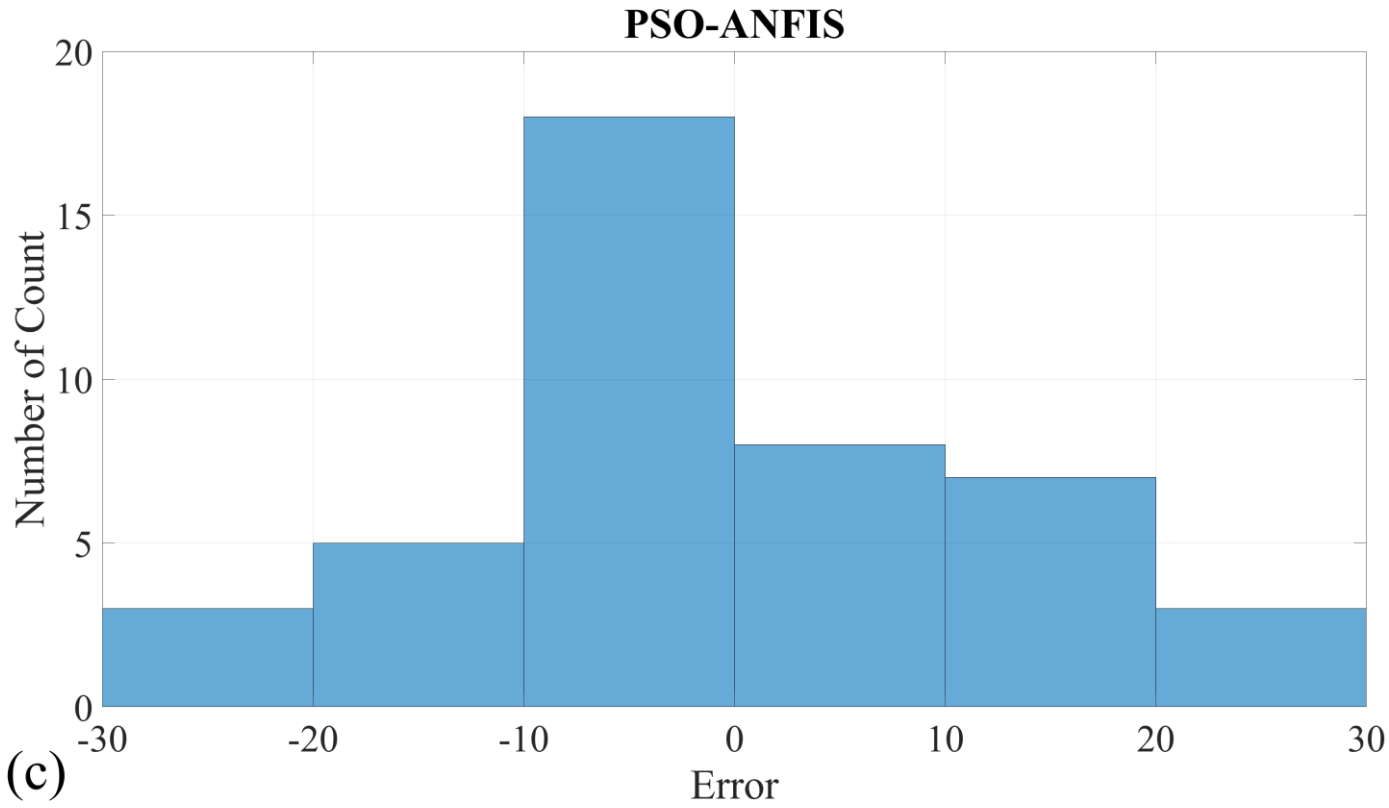
Fig. 12. The error histogram of the data during training and testing using (a): GP; (b): GA-ANFIS; (c): PSO-ANFIS; (d): GWO-ANFIS; (e): B-ANFIS.



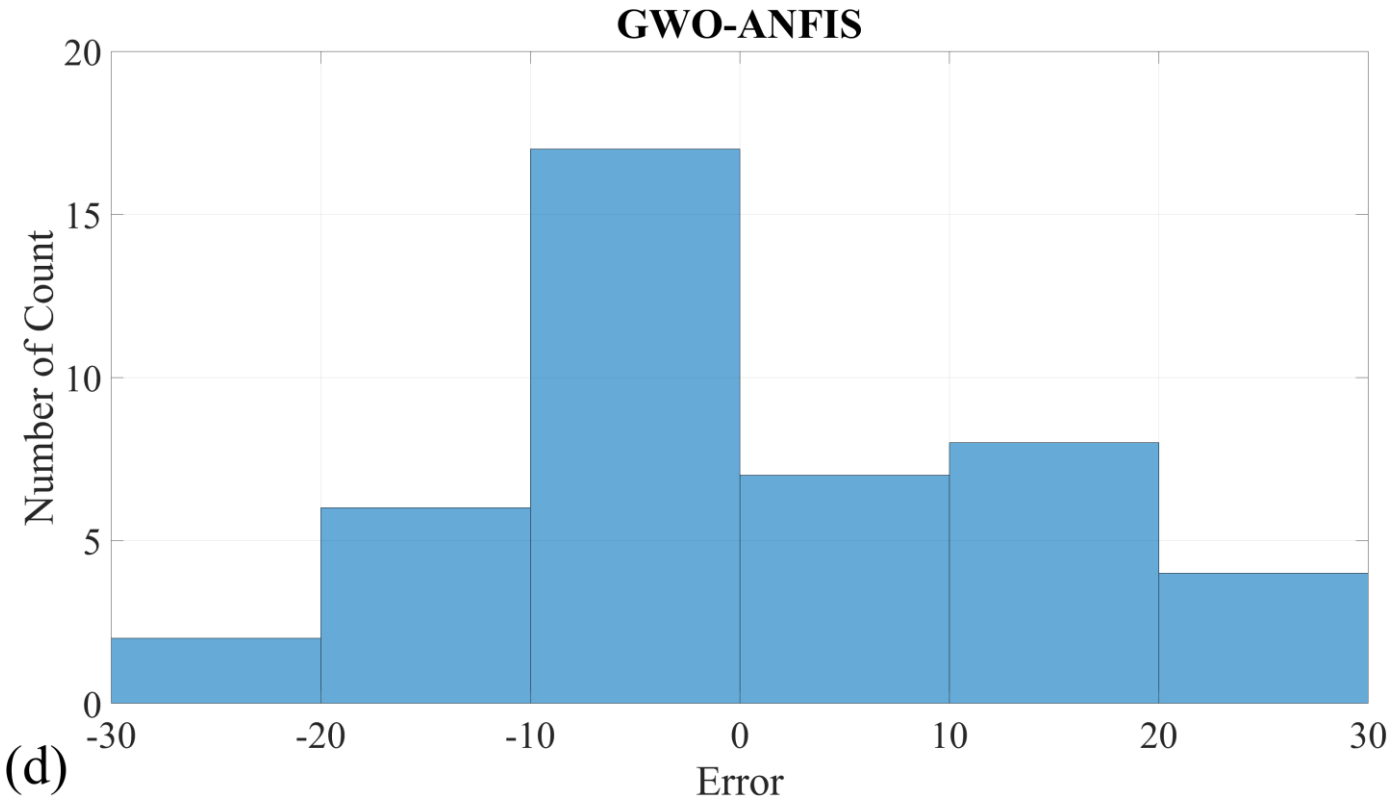
(a)



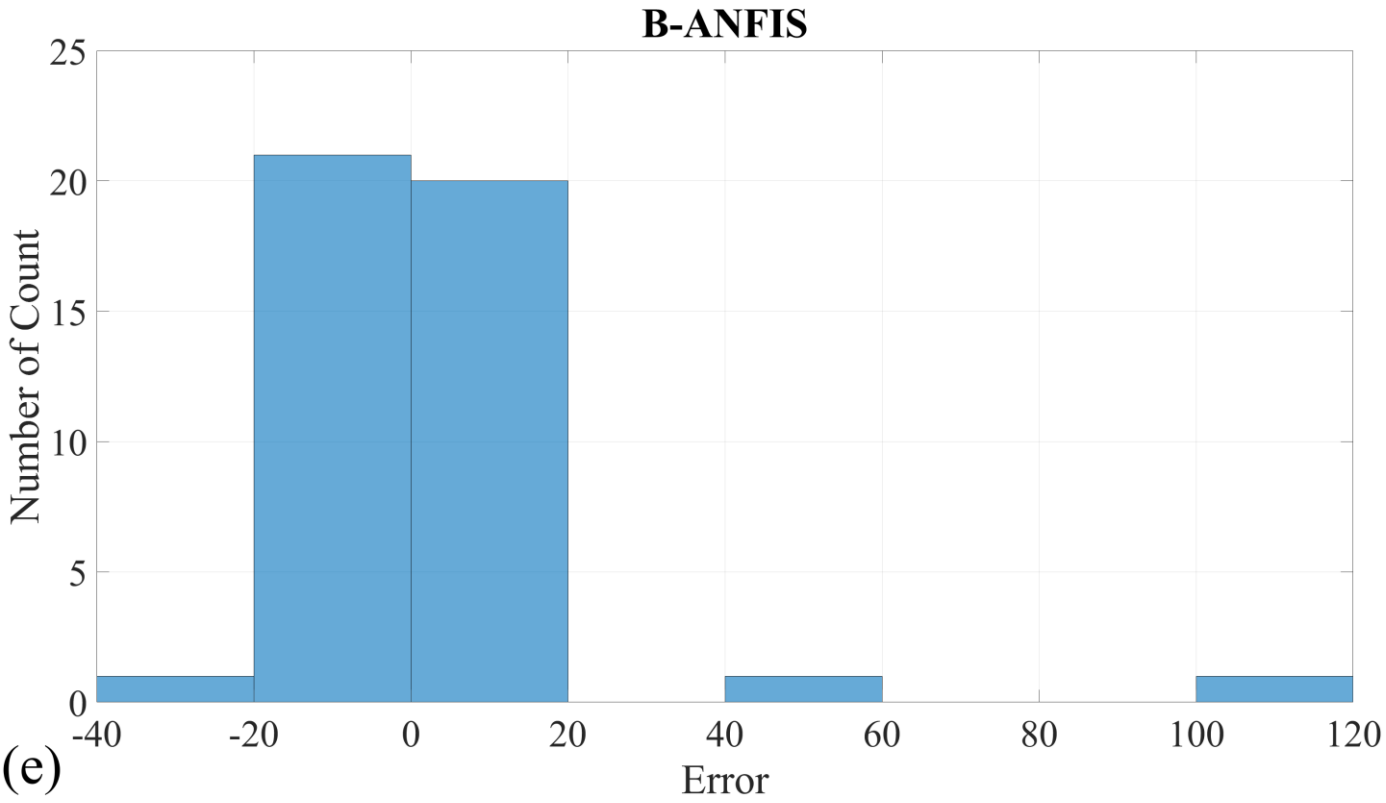
(b)


PSO-ANFIS
Number of Count
Error
0
5
10
15
20
-30
-20
-10
0
10
20
30

(c)

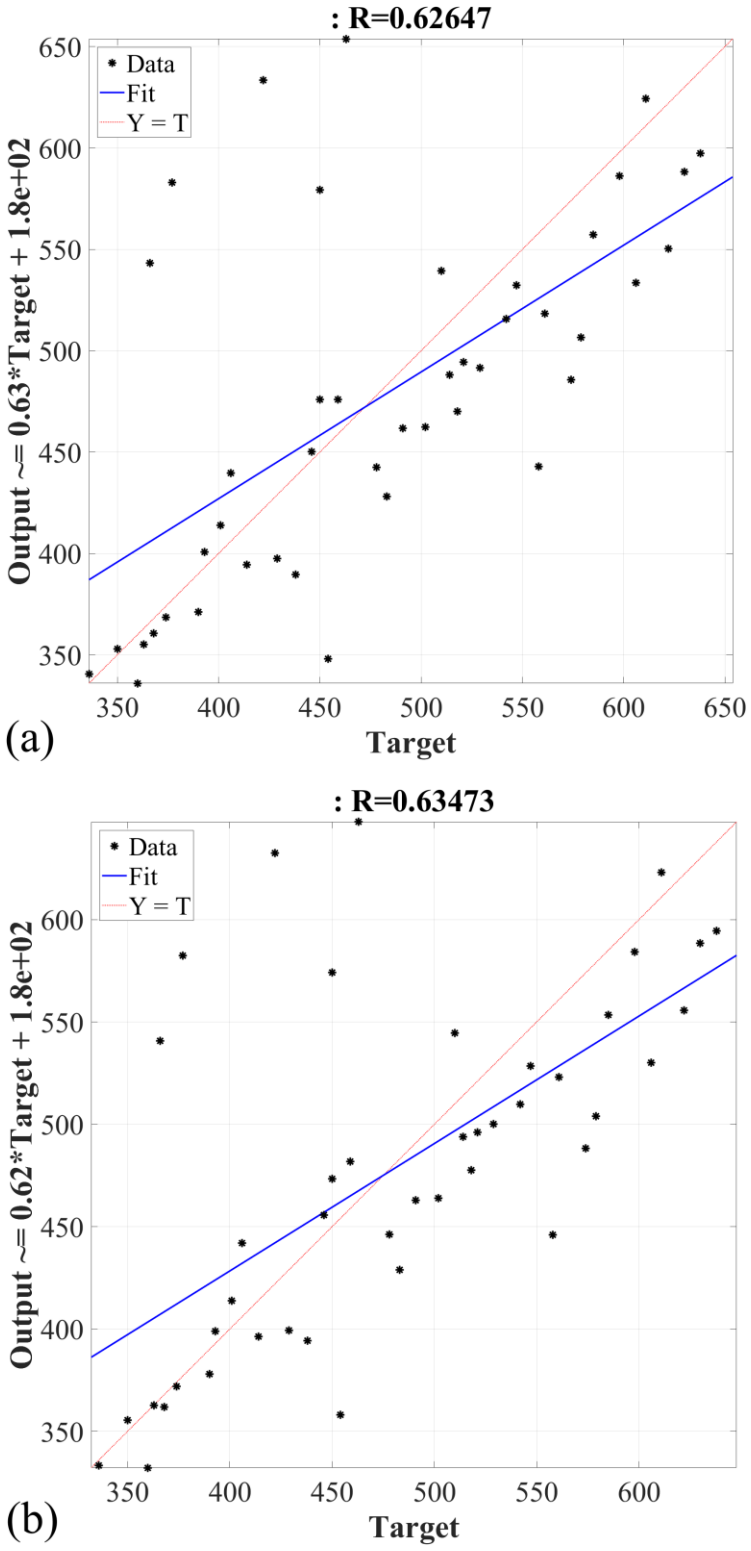

GWO-ANFIS
Number of Count
Error
0
5
10
15
20
-30
-20
-10
0
10
20
30

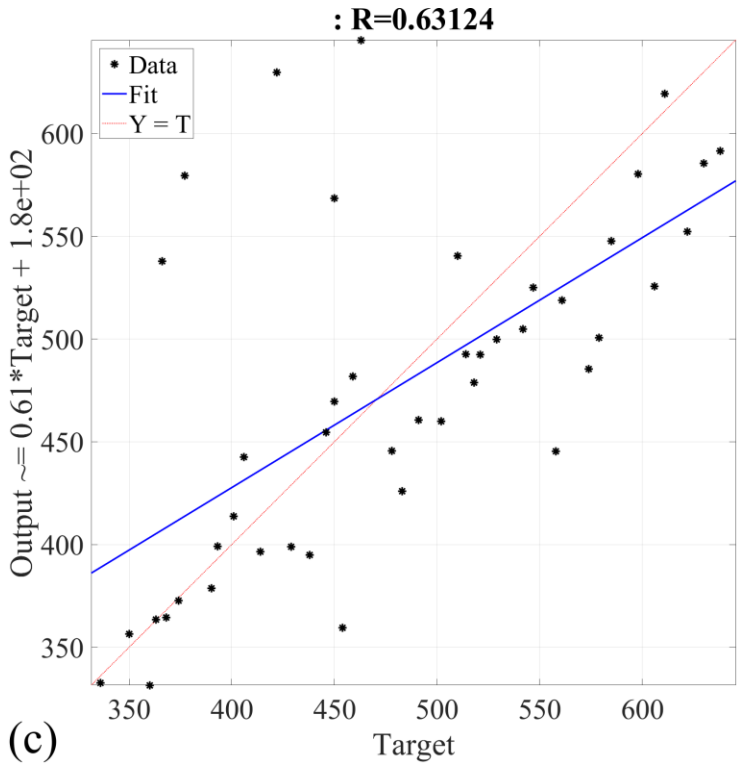
(d)


B-ANFIS
Number of Count
Error
25
20
15
10
5
0
-40
-20
0
20
40
60
80
100
120

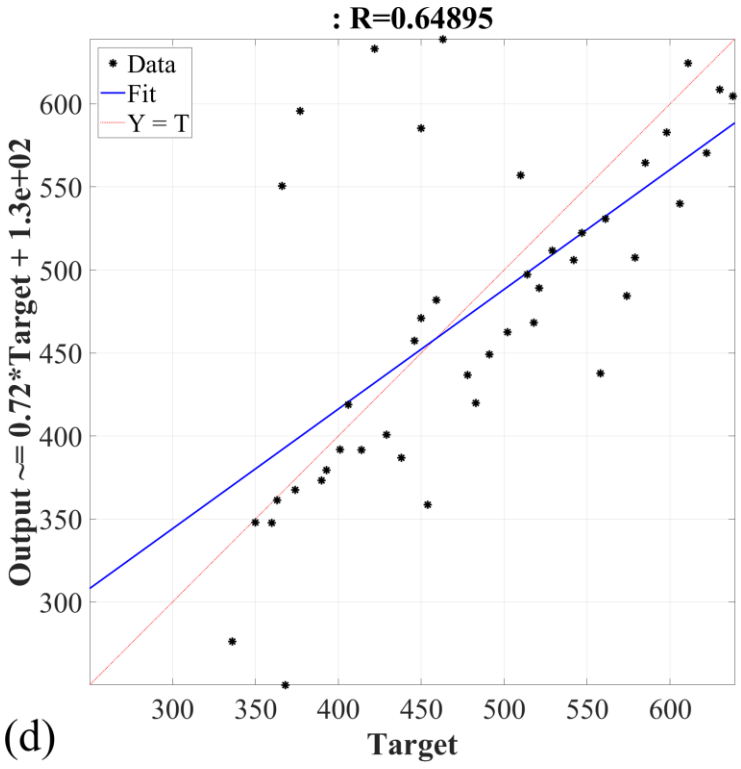
(e)

Fig. 13. The regression representation of the data during training and testing using (a): GA-ANFIS; (b): PSO-ANFIS; (c): GWO-ANFIS; (d): B-ANFIS.




: R=0.63124
Data
Fit
Y = T
Output ~= 0.61*Target + 1.8e+02
Target
350
400
450
500
550
600

(c)


: R=0.64895
Data
Fit
Y = T
Output ~= 0.72*Target + 1.3e+02
Target
300
350
400
450
500
550
600

(d)

TABLE 1
Design of experiments table for the testing purpose of the algorithm.

a (mm)	2.7	2.4	2.1	1.8	1.5
f (mm/rev)	0.19	0.16	0.13	0.10	0.07
v (m/min)	160	140	120	100	80

TABLE 2
The selected hyperparameter of ANFIS using four optimization methods.

ITEM	**Initial FIS**	**Epoch Number**	**Initial Step Size**	**Step Size Decrease Rate**	**Step Size Increase Rate**
GA	2	31	0.0902	0.6814	1.1622
PSO	2	25	0.1	0.5842	1.3559
GWO	2	26	0.0819	0.5753	1.4945
Bayesian	2	130	0.0985	0.5128	1.0033

TABLE 3
The obtained results using GP, GA-ANFIS, PSO-ANFIS, GWO-ANFIS, and B-ANFIS.

row	Mode	Iso	*v*	*ẏf*	*a*	Exp	Model GP	GA-ANFIS	PSO-ANFIS	GWO-ANFIS	B-ANFIS
1	Training	A1	100	0.07	1.5	358	401.7814074	348.0692565	**358.1054051**	359.4504582	358.7610203
2		A2	110	0.15	1.5	454	489.7417479	450.166777	455.7565333	**454.5418007**	457.3535632
3		A3	120	0.11	1.5	446	416.6516714	461.6611226	463.0137841	460.5410703	**449.0993922**
4		A4	120	0.13	1.5	491	432.2887874	494.4341912	496.2303222	**492.5315976**	489.1016034
5		A5	130	0.11	1.5	521	496.3993776	532.2108038	528.4502497	525.0891199	**522.3676476**
6		A6	140	0.09	1.5	547	514.9351992	543.1905559	540.8620154	537.8026924	**550.5393662**
7		B1	100	0.09	1.8	366	401.6559088	368.5034851	371.9656429	372.7322914	**367.6950194**
8		B2	110	0.07	1.8	374	340.6535805	371.1952136	378.0040179	378.6254049	**373.4031081**
9		B3	110	0.09	1.8	390	424.0948915	**389.6622545**	394.2503381	394.942957	**387.0459081**
10		B4	110	0.13	1.8	438	460.8753311	442.9349002	445.9473379	445.4599787	**437.8445515**
11		B5	120	0.15	1.8	558	591.2439494	539.3505874	544.6724015	540.4454456	**557.0844215**
12		B6	130	0.09	1.8	510	469.417515	506.6137516	503.9069629	500.7098948	**507.3757421**
13		B7	130	0.13	1.8	579	562.1979545	586.2932368	584.2485526	**580.367747**	582.8313611
14		B8	140	0.11	1.8	598	560.6885547	583.0190763	582.4205869	579.4607065	**595.6831203**
15		C1	100	0.11	2.1	377	342.6538818	400.8367031	399.0111633	399.0056736	**379.5077038**
16		C2	110	0.09	2.1	393	401.9334642	394.5096371	396.35366	396.4152901	**391.6980143**
17		C3	120	0.07	2.1	414	462.1326326	428.0566888	428.9138142	425.9032456	**419.825271**
18		C4	120	0.11	2.1	483	534.6677819	485.7012625	488.1879469	485.3700706	**484.453729**
19		C5	120	0.15	2.1	574	537.4129947	550.2905289	555.7699798	552.4151261	**570.4354865**
20		C6	130	0.15	2.1	622	647.1607008	624.3668307	**623.0718871**	619.4436783	624.4269583
21		C7	140	0.11	2.1	611	580.3684866	588.346405	588.4031674	585.5753615	**608.7311728**
22		C8	140	0.13	2.1	630	650.6027694	633.4130535	632.5444646	**629.8756533**	633.1225557
23		D1	100	0.13	2.4	422	458.77847	439.7053548	442.0190871	442.5479064	**418.8214176**
24		D2	110	0.09	2.4	406	459.2997775	397.5007666	399.4101489	398.929306	**400.7518295**
25		D3	110	0.11	2.4	429	462.2534908	442.5738803	446.18339	445.4775983	**436.7196805**
26		D4	110	0.13	2.4	478	440.2174528	**475.9582676**	481.8026434	481.78181	481.969444
27		D5	120	0.09	2.4	459	478.8746948	462.2736957	463.9835046	**460.0884554**	462.4902335
28		D6	130	0.07	2.4	502	470.3657442	515.722535	509.8285109	**504.7779029**	506.0230214
29		D7	130	0.09	2.4	542	499.6224009	533.4539022	530.0889719	525.6372951	**539.9591706**
30		D8	130	0.13	2.4	606	540.5400762	597.4402204	594.4633472	591.6042995	**604.7567125**
31		D9	140	0.15	2.4	638	600.6828371	653.8200528	647.7510859	645.5456371	**639.0398527**
32		E1	100	0.15	2.7	463	423.0474159	469.9834934	477.7035675	478.7533533	**468.1665351**
33		E2	110	0.13	2.7	518	561.9491219	491.5301843	500.1071442	499.8505901	**511.5803675**
34		E3	120	0.11	2.7	529	559.750999	518.2656546	523.000733	518.7960625	**530.7042118**
35		E4	130	0.09	2.7	561	596.6019093	557.3071013	553.4885547	547.7675645	**564.6303026**
36		E5	140	0.07	2.7	585	549.4620441	579.400494	574.1487175	568.5215497	**585.2994368**
37	Testing	T1	125	0.08	2.1	450	481.0345025	475.9210273	473.4145114	**469.6744777**	470.884835
38		T2	115	0.12	2.4	514	579.5498717	488.1132334	493.9729125	492.5654231	**497.398716**
39		T3	90	0.08	2.4	360	328.6387066	335.9821749	332.2415647	331.511809	**347.7967525**
40		T4	55	0.2	2.7	368	300.0443233	360.6337183	361.9184017	**364.4886874**	250.141412
41		T5	105	0.12	1.8	401	480.9418007	414.0190118	413.8109028	413.7408843	**391.9964342**
42		T6	107	0.06	1.8	363	398.9776764	355.0705525	**362.7671665**	363.4757113	361.4737095
43		T7	90	0.1	1.5	350	300.3815161	352.9666644	355.4669756	356.4550555	**347.962778**
44		T8	80	0.12	1.5	336	280.7085504	340.5188007	**333.3495407**	332.6240653	276.307393

TABLE 4
The selected hyperparameter of ANFIS using four optimization methods.

Model	Process	MSE	RMSE	NRMSE	Mean Error	STD	CC	R2
GP	Training	1.38E+03	37.1975	0.0745	1.4165	37.6978	0.4483	0.4674
	Testing	3.01E+03	54.8471	0.1426	-1.0346	58.6236	0.9234	0.8571
GA-ANFIS	Training	142.5936	11.9413	0.0239	0.3955	12.104	0.4697	0.4996
	Testing	279.3417	16.7135	0.0426	2.3469	17.6905	0.958	0.9286
PSO-ANFIS	Training	127.3116	11.2832	0.0226	-0.8908	11.4076	0.4745	0.5042
	Testing	244.7408	15.6442	0.0398	1.8823	16.6029	0.9644	0.9048
GWO-ANFIS	Training	149.8221	12.2402	0.0245	1.256	12.3483	0.4693	0.503
	Testing	235.7567	15.3544	0.0391	2.183	16.2478	0.9648	0.9286
Bayesian-ANFIS	Training	10.804	3.2869	0.0066	-0.7583	3.2436	0.4884	0.4973
	Testing	2.30E+03	47.961	0.1221	24.7547	43.915	0.8732	0.7381